Applied Geochemistry 91 (2018) 75–88

Contents lists available at ScienceDirect

Applied Geochemistry

journal homepage: www.elsevier.com/locate/apgeochem

Speciation dynamics of oxyanion contaminants (As, Sb, Cr) in argillaceous suspensions during oxic-anoxic cycles

Ekaterina Markelova[a,b,*], Raoul-Marie Couture[b,c], Christopher T. Parsons[b], Igor Markelov[a,b], Benoit Madé[d], Philippe Van Cappellen[b], Laurent Charlet[a,b]

[a] University Grenoble Alpes, University Savoie Mont Blanc, CNRS, IRD, IFSTTAR, ISTerre, 38000 Grenoble, France
[b] Ecohydrology Research Group, Department of Earth and Environmental Sciences and Water Institute, University of Waterloo, 200 University Ave. W, Waterloo, ON N2L 3G1, Canada
[c] Norwegian Institute for Water Research-NIVA, Gaustadalléen 21, 0349 Oslo, Norway
[d] Andra, National Radioactive Waste Management Agency, R&D Division, Transfer Migration Group, 1/7 rue Jean Monnet, 92298 Chatenay Malabry Cedex, France

ARTICLE INFO

Keywords:
Argillaceous suspension
Nuclear waste repository
Redox oscillations
Arsenic
Antimony
Chromium
Sequestration
Reduction
Respiration
Detoxification

ABSTRACT

Argillaceous geological formations are considered promising repositories for waste containing inorganic contaminants. However, the sequestration capacity of an argillaceous natural barrier may change as a result of dynamic environmental conditions, in particular changes in redox state. Here, we imposed redox cycles to argillaceous suspensions amended with a mixture of the inorganic contaminants As(V), Sb(V), Cr(VI), by alternating 7-day cycles of sparging with either oxic or anoxic gas mixtures. During the redox cycles, we assessed the relative importance of different contaminant sequestration mechanisms under sterile and non-sterile conditions. The non-sterile experiments were carried out 1) with the argillaceous material as is, that is, containing the native microbial population, 2) with the addition of ethanol as a source of labile organic carbon, and 3) with the addition of both ethanol and a soil microbial inoculum. In order to capture the observed solid-solution partitioning trends, a series of mixed thermodynamic-kinetic models representing the dynamic conditions in the experiments were developed using PHREEQC. Parameter values for processes such as adsorption, which occurred in all experiments, were kept constant across all the simulations. Additional formulations were introduced as needed to account for the microbial detoxification and respiration of the contaminants in the increasing complexity experiments. Abiotic adsorption of As and abiotic reductive precipitation of Cr dominated sequestration of these two contaminants under all experimental conditions, whereas the presence of microorganisms was essential to decrease the aqueous Sb concentration. Once reduced, As(III), Sb(III), and Cr(III) were not re-oxidized upon exposure to dissolved O_2 in any of the experiments. Neither the mineralogy nor the native microbiota catalysed contaminant oxidation processes. Thus, kinetically, the reduction of As(V), Sb(V), and Cr(VI) was irreversible over the experimental duration (49 days). The capacity of the argillaceous matrix to reduce and sequester the aqueous contaminants, without subsequent remobilization to the aqueous phase during the oxic periods, supports the use of argillaceous barriers for geologic waste storage.

1. Introduction

Argillaceous formations are being investigated as potential geological hosts for radioactive waste disposal in eleven Nuclear Energy Agency member countries, which are collectively referred to as the Clay Club (Nuclear Energy Agency, 1958). In low-level radioactive waste (e.g., long-lived radium-bearing waste) potentially toxic elements, including As, Sb, and Cr, are often present in addition to radionuclides, and may be released into the argillaceous porous media if failure of engineered barriers occurs (Andra, 2009). Furthermore, these contaminants are of general geochemical interest as they are often released to near-surface environments due to industrial pollution adjacent to mining and smelting operations (Cornelis et al., 2008; Wilson et al., 2010), shooting ranges (Johnson et al., 2005), and chemical weathering of natural rocks and minerals (e.g., pyroxenite, serpentinite, arsenopyrite, scorodite, stibnite; Godgul and Sahu, 1995; Wilson et al., 2010).

The mobility, bioavailability, and chemical reactivity of redox-sensitive As, Sb, and Cr are influenced by their speciation, which evolves

* Corresponding author. University Grenoble Alpes, University Savoie Mont Blanc, CNRS, IRD, IFSTTAR, ISTerre, 38000 Grenoble, France.
E-mail addresses: emarkelo@uwaterloo.ca, ekaterina.markelova@ujf-grenoble.fr (E. Markelova), rmc@niva.no (R.-M. Couture), chris.parsons@uwaterloo.ca (C.T. Parsons), igor.markelov@uwaterloo.ca (I. Markelov), Benoit.Made@andra.fr (B. Madé), pvc@uwaterloo.ca (P. Van Cappellen), laurent.charlet@ujf-grenoble.fr (L. Charlet).

https://doi.org/10.1016/j.apgeochem.2017.12.012
Received 12 July 2017; Received in revised form 12 December 2017; Accepted 13 December 2017
Available online 15 December 2017

according to changes in redox conditions, pH, electrolyte composition, temperature, and microbial activity (e.g., Fawcett et al., 2015). At near-neutral pH, oxidized species are expected to be present as oxyanions (primarily $HAsO_4^{2-}$, $Sb(OH)_6^-$, and CrO_4^{2-}) with low sorption affinity to typically negatively charged clay surfaces dominant in an argillaceous matrix. Therefore, similarly to radionuclides, which may be present in anionic forms (e.g., Br, I) (Tournassat et al., 2007; Wersin et al., 2011), the potentially toxic contaminants As, Sb and Cr are of concern for waste management due to their expected mobility in the absence of positively charged Fe- or Al-oxide minerals (Manning and Goldberg, 1997; Zhang and Selim, 2005).

Dynamic changes in redox conditions have significant effects on aqueous contaminant concentrations in saturated near-surface environments (Couture et al., 2015; Hindersmann and Mansfeldt, 2014; Parsons et al., 2013; Stewart et al., 2009; Thompson et al., 2006), suggesting that they also play a role in controlling contaminant mobility in subsurface argillaceous formations. Research on how redox phenomena control the long-term mobility of radionuclides in waste repositories has been performed by 32 European research institutes and universities within the ReCosy collaborative project (Duro et al., 2014). However, in contrast to radionuclides, the mobility of associated metals and metalloids has received much less attention in waste management research.

Most of the experimental and modelling investigations assessing the long-term performance of geological repositories assume that highly reducing conditions develop and are maintained after repository closure (e.g., Hedin and Olsson, 2016; Laaksoharju et al., 2008). The assumption of stable reducing conditions may not always hold since oxidizing conditions can last from a few years to a hundred years during the initial period of repository utilization (Bildstein et al., 2005; Duro et al., 2014; Nagra, 2002; Stroes-Gascoyne et al., 2002). The intrusion of oxygenated groundwater (Swift and Bonano, 2016) or glacial melt water (Duro et al., 2014; Laaksoharju et al., 2008), as well as water radiolysis (Rodwell et al., 2003; Song and Zhang, 2008) are further potential causes of redox perturbations over the life-time of the repository. Therefore, the examination of natural barrier materials in contact with potentially toxic contaminants under redox-oscillating conditions can help inform scenarios of repository safety.

Besides the potential role of the redox conditions, contaminant mobility within repositories can be altered by the presence of microorganisms, which are commonly found to depths of at least 1500 m (Pedersen, 2002). In fact, microbial activity plays an important role in shaping geochemical processes even in deep, low-nutrient environments, such as granitic bedrock (Laaksoharju et al., 2008), and thus should not be ignored in environmental assessments of future repositories. A number of safety assessments already incorporate microbial processes into the predictive modelling of repository conditions (e.g., Hallbeck and Pedersen, 2012; Laaksoharju et al., 2008; Small et al., 2008). Prediction of contaminant mobility influenced by microbial activity should also be implemented.

The high heterogeneity of waste materials complicates environmental assessments, in particular when multiple contaminants are present in a mixture of coexisting redox-sensitive elements. Contaminated soils and waste waters are often found to contain high concentrations of As, Sb, and Cr as well as redox-sensitive nutrients, such as nitrogen (N) and organic carbon (OC) (Casiot et al., 2007; Hindersmann and Mansfeldt, 2014; Lindsay et al., 2011). Heterogeneous contaminant-nutrient mixtures are also prevalent in waste repositories (Bertron et al., 2014). Given that the biogeochemical cycles of nutrients and contaminants are intricately linked together (Andrewes et al., 2000; Couture et al., 2015; Stucker et al., 2014), there is a need for investigating multi-contaminant mixtures more systematically.

In this study, we evaluate the mobility of oxidized oxyanion contaminants ($HAsO_4^{2-}$, $Sb(OH)_6^-$, and CrO_4^{2-}) in argillaceous suspensions under a range of variable environmental conditions. We present the results of a series of batch experiments focusing on the effects of oxic *vs.* anoxic and biotic *vs.* abiotic conditions in bioreactors. The role of adding labile OC (ethanol) as an electron donor, and the effect of microbial diversity are also evaluated. We hypothesized that (1) reintroduction of O_2 in the argillaceous suspension would increase contaminant mobility via oxidation of reduced compounds, (2) increased heterotrophic microbial activity and ethanol addition would decrease contaminant mobility by increasing reductive precipitation of Sb and Cr, and (3) the contaminants would be reduced sequentially following the order of decreasing redox potential of the corresponding reduction reactions.

In the experiments, the complexity of the reactive systems was progressively increased. Observed geochemical patterns were interpreted using mixed kinetic-thermodynamic models that incorporated an increasing number of reaction pathways. Parameter values obtained for processes in simpler systems were fixed and applied unchanged in models of more complex systems, hence allowing us to assess the transferability of the reaction parameters. The models provide diagnostic and prognostic tools for the quantitative simulation of biogeochemical processes driving the partitioning of As, Sb, and Cr in argillaceous systems.

2. Materials and methods

2.1. Argillaceous matrix, synthetic pore water, and contaminant mixture

A sample of Tégulines argillaceous material from the Gault formation in north-eastern France was collected at 22.5 m depth and preserved under anaerobic conditions prior to use. The initial mineral composition of the argillaceous matrix was characterised by powder X-ray diffraction (XRD) using a Bruker Axs D8 diffractometer. Prior to analysis, the sample was dried undisturbed under an O_2-free atmosphere in an anaerobic chamber (Jacomex BS 531, EP20Ra-nm purification, 100% N_2, < 1 ppm O_2) and ground by hand in an agate mortar to a particle size of approximately 1–3 µm. Diffractograms were obtained using a Cu-target X-ray tube analysing $K\alpha_{1+2}$ lines with a solXE detector. The X-ray diffraction patterns were treated by Rietveld refinement using BGMN software (Bergmann et al., 1998). Elemental composition was determined by inductively coupled plasma optical emission spectrometry (ICP-OES) (Varian 720 ES) after total acid digestion (HNO_3 + HF + H_3BO_3 + H_2O_2) (Cotten et al., 1995). Concentrations of reducible Fe and Mn, as well as those of reactive, Al were estimated by performing citrate-bicarbonate-dithionite (CBD) extractions (Jackson et al., 1986).

After grinding, the argillaceous sample was sieved through a 1 mm mesh, dispersed in synthetic pore water (50 g L^{-1}) and equilibrated, with agitation, for 7 days under O_2-free conditions prior to oxyanion additions. The synthetic pore water (Table B.1) mimicked the solution composition in contact with the host rock formation in the absence of O_2 (Gaucher et al., 2009). It was enriched in NO_3^- and NH_4^+ in order to simulate the leachate of a bitumen matrix (Bertron et al., 2014). The oxyanion mixture was prepared by dissolving high purity analytical grade $Na_2HAsO_4{\cdot}7H_2O$ (≥ 98%, SIGMA), $KSb(OH)_6$ (≥ 99%, Fluka), and K_2CrO_4 (≥ 99%, SIGMA-ALDRICH). Individual stock solutions of As and Cr were combined and added to the pre-equilibrated experimental suspensions, while Sb was spiked separately to prevent precipitation of $NaSb(OH)_6$ due to the high stock concentration of Na (Ilgen et al., 2014).

2.2. Experiments

Batch experiments were performed using a bioreactor system based on the design of Thompson et al. (2006) and modified by Parsons et al. (2013). Briefly, each reactor contained a suspension volume of 1 L with a headspace of about 300 ml and incubated in the dark. Electrodes, mechanical agitator, and sampling ports were installed via the reactor head-plate while a water jacket ensured constant temperature

(25 ± 1 °C). Solid polymer open junction pH and redox potential (E_H) electrodes (Mettler-Toledo Xerolyt Solid) were connected to field-effect transistor (FET) instrumental amplifiers with high input impedance. The E_H and pH data were recorded every 2 min using an Agilent 34970A Data Logger. Measured E_H was corrected for the reference electrode's standard voltage (+207 mV) relative to the standard hydrogen electrode (SHE) at 25 °C and referred to a Ag/AgCl (3 M KCl) reference electrode.

Experimental time zero corresponds to the time of injection of the oxyanion mixture to a pre-equilibrated suspension under anoxic conditions. Redox oscillations were induced by alternate sparging of anoxic (1% CO_2 + 99% N_2) and oxic (1% CO_2 + 79% N_2 + 20% O_2) gas mixtures for periods of 7 days for a total experimental time of 7 weeks. Sampling was performed on the 1st, 2nd, 4th, and 7th day of each anoxic and oxic period using gas-tight sterile syringes. Suspensions were subsampled, immediately centrifuged, and filtered through cellulose hydrophilic membrane filters (0.2 µm pore size, Chromafil RC, ROTH) in the anaerobic chamber. A part of the supernatant was flash frozen with liquid nitrogen and stored at −80 °C prior to aqueous speciation analysis. The rest of the supernatant was acidified with ultrapure HNO_3 to pH < 3 and stored at 4 °C for total aqueous concentration analyses.

Each batch experiment included the Tégulines argillaceous material and the synthetic pore water (Table B.1) amended with the oxyanion mixture. The targeted initial contaminant concentrations were 500 µM $HAsO_4^{2-}$, 500 µM $Sb(OH)_6^-$, and 500 µM CrO_4^{2-} (Table B.2). In total, four increasing complexity experiments were performed (Table 1) to identify the respective contributions of argillaceous mineralogy (Exp. I), native microbial community (Exp. II), ethanol addition (Exp. III), and microbial enrichment (Exp. IV) on the fate of the added As(V), Sb (V) and Cr(VI) under oscillating oxic-anoxic conditions.

Specifically, Exp. I was performed as an abiotic control created by sterilizing the argillaceous material at 121 °C for 15 min prior to the experiment and by adding microbial inhibitors (Na-azide, streptomycin, and kanamycin sulphates from Sigma-Aldrich) to the experimental suspension. Exp. II was performed with the argillaceous suspension without additional treatment. In Exp. III, 20 mM of dissolved organic carbon (DOC) as ethanol (≥99.8%, SIGMA-ALDRICH) was added at the beginning of each anoxic period as a source of labile OC (Wu et al., 2007). In Exp. IV, the native microbial community was enriched by adding a soil inoculum (See Appendix C), while also adding ethanol as in Exp. III. The inoculum was extracted from a natural floodplain soil located in a zone experiencing frequent redox fluctuations. Previous characterization of the microbial ecology at this field site demonstrated the presence of a broad diversity of aerobic and anaerobic bacteria (Parsons et al., 2013). Details on the preparation and injection of soil inoculum are given in Annex C.

2.3. Analyses

All standards and reagents were of analytical grade and all solutions were prepared in Milli-Q water (resistivity 18.2 MΩ cm^{-1}). Anion concentrations (NO_3^-, NO_2^-, SO_4^{2-}, Cl^-, and $C_2H_3O_2^-$) were determined by ion chromatography (Metrohm 761 Compact IC); total aqueous concentrations of Na, K, Ca, Mn, Fe, S, As, Cr, Sb were measured by ICP-OES (Varian 720 ES). Certified multi-elemental solutions (Sigma-Aldrich) were used for quality control with measured concentrations always within 10% of the certified values. Hereafter, we refer to aqueous concentrations using square brackets.

A UV–Vis spectrophotometer (Agilent 8453E UV–Visible) was used to measure the aqueous speciation of Cr by recording absorbance at 272 and 373 nm (Rai et al., 2007; Zydorczak et al., 2012). Speciation of aqueous Sb was measured by high performance liquid chromatography (HPLC) coupled to ICP-OES according to Lintschinger et al. (1997). Briefly, a Hamilton anion exchange column (PRP-X100, 4.1 9150 mm, 10 mm) was used with a mobile phase of 20 mM EDTA (Fluka) and 2 mM KHP (Sigma-Aldrich) (pH 4.3) at a flow rate of 1.5 ml min^{-1} for the separation of Sb(V) and Sb(III) peaks. Aqueous speciation of As(V) and As(III) was performed using the same column with a mobile phase of KH_2PO_4:K_2HPO_4 (Merck) at pH 6.25 prior to analysis by ICP-OES (Roig-Navarro et al., 2001).

Solid-phase concentrations of oxidized As, Sb, and Cr were determined on samples collected on the last day of each experiment. The samples were analysed by ICP-OES after leaching with a 0.1 M Na_2CO_3 solution (Panichev et al., 2005). The alkaline extraction is assumed to selectively release the oxidized species of As, Sb and Cr. Concentrations of reduced As, Sb, and Cr species were estimated by difference between total concentrations after acid digestion and concentrations measured in the Na_2CO_3 extracts (Panichev et al., 2005).

Dissolved inorganic carbon (DIC) and DOC concentrations were determined on a carbon analyser (Shimadzu TOC-Vcsn). Further characterization of DOC was performed by measuring the raw absorbance at 254 nm and calculating specific UV absorbance (SUVA 254) (Cory and McKnight, 2005). Microbial activity was inferred from temporal trends in nitrate (NO_3^-) and adenosine triphosphate (ATP) concentrations (e.g., Hammes et al., 2010; Karl, 1980). The ATP concentrations were determined by measuring luminescence levels (Lumat LB 9507 Berthold Technologies) after application of a BacTiter-Glo Microbial Cell Viability Assay kit (Promega).

Table 1
Design of batch experiments comprising the Tégulines sample (50 g L^{-1}) dispersed in 1 L of synthetic pore water (Table B.1) and amended with a mixture of As(V), Sb(V), and Cr (VI).

Factors tested	Exp. I	Exp. II	Exp. III	Exp. IV
Sterile mineralogy	+	+	+	+
Microbial activity of native community		+	+	+
Labile organic carbon (ethanol) addition			+	+
Microbial activity of enriched (native + inoculated) community				+

2.4. Biogeochemical modelling

Biogeochemical modelling was designed to identify key reactive processes and limiting factors controlling the behaviour of As, Sb and Cr during the experiments, by reproducing observed the contaminant speciation and concentration time series data. An increasing complexity modelling approach was used: parameter values derived in an earlier (simpler) experiment were fixed and used unchanged in the models for the subsequent (more complex) experiments.

Contaminant fate in the least complex experiment (Exp. I) was quantitatively assessed by fitting the multi-reaction model of Zhang and Selim (2005) to the time series of As, Sb, and Cr concentrations. The numerical solution was obtained by solving a set of nonlinear differential and algebraic equations (see detailed model description in Appendix D) in PHREEQC v.3.1.7 (Parkhurst and Appelo, 2013). The model simulates cycles of oxic and anoxic conditions by alternating the equilibrium headspace composition controlled by $O_{2(g)}$ (0.2 atm) and $CO_{2(g)}$ (0.01 atm), respectively. Equilibrium with pCO_2 and calcite was imposed to buffer the pH. The WATEQ4F database was used as a starting point and additional equilibrium constants from the literature were used as required (Table D.1, D.2).

The multi-reaction model for Exp. I was run for each of the three contaminants to derive parameter values for the reversible equilibrium sorption constant (K_{eq}), the rate constants for reversible adsorption (k_f) and desorption (k_b), plus the rate constant for irreversible sorption (k_i). The model for Exp. II incorporated all reactions used for Exp. I, supplemented by microbially driven reduction reactions with rates formulated based on modified Monod kinetics (e.g., Van Cappellen and Wang, 1996). Chemical and microbial reactions were assumed to occur in parallel. No changes to the model of Exp. II were required to reproduce contaminant behaviour in Exp. III. Finally, the most complex

Table 2
Reaction network and kinetic formulations used in the biogeochemical models. Parameter values are given in Annex D (Table D.2).

Description	Reaction	Kinetic or equilibrium formulation	R#
Electrode leakage		$R_1 = r_{leak}^{DOC}$	1
Fermentation of ethanol	$C_2H_5OH + H_2O \rightarrow CH_3COO^- + 5\,H^+ + 4\,\bar{e}$	$R_2 = k^{C_2H_5OH}\cdot[C_2H_5OH]\cdot\left(\frac{K_{in}^{O_2}}{K_{in}^{O_2}+[O_2]}\right)$	2
Fermentation of acetate	$CH_3COO^- + 4\,H_2O \rightarrow 2\,HCO_3^- + 9\,H^+ + 8\,\bar{e}$	$R_3 = k^{CH_3COO^-}\cdot[CH_3COO^-]\cdot\left(\frac{K_{in}^{O_2}}{K_{in}^{O_2}+[O_2]}\right)$	3
Aerobic respiration of ethanol	$O_2 + C_2H_5OH \rightarrow CH_3COO^- + H_2O + H^+$	$R_4 = k_{eth}^{O_2}\cdot[C_2H_5OH]\cdot\left(\frac{[O_2]}{[O_2]+K_m^{O_2}}\right)$	4
Aerobic respiration of acetate	$2\,O_2 + CH_3COO^- + H^+ \rightarrow 2\,CO_2 + 2\,H_2O$	$R_5 = k_{ac}^{O_2}\cdot[CH_3COO^-]\cdot\left(\frac{[O_2]}{[O_2]+K_m^{O_2}}\right)$	5
Arsenic			
Equilibrium adsorption of As(V)	$HAsO_4^{2-} + 2\,{\equiv}SOH \rightleftarrows {\equiv}SOHAsO_4 + H_2O$	$logK_{sorp}^{HAsO_4^{2-}}$	6
Kinetic sorption of As(V)	$HAsO_4^{2-} + 2\,{\equiv}SOH \rightleftarrows {\equiv}SOHAsO_4 + H_2O$	$R_f^7 = k_f^{HAsO_4^{2-}}\cdot[HAsO_4^{2-}]$	7
		$R_b^8 = k_b^{HAsO_4^{2-}}\cdot{\equiv}SOHAsO_4$	8
		$R_i^9 = k_i^{HAsO_4^{2-}}\cdot{\equiv}SOHAsO_4$	9
Detoxification of aqueous As(V)	$HAsO_4^{2-} + 4\,H^+ + 2\,\bar{e} \rightarrow H_3AsO_3 + H_2O$	$R_{detox}^{10} = r_{max}^{HAsO_4^{2-}}\cdot\left(\frac{[HAsO_4^{2-}]}{K_{m\,(detox)}^{HAsO_4^{2-}}+\left[HAsO_4^{2-}\right]}\right)$	10

Description	Reaction	Kinetic or equilibrium formulation	R#
Respiration of aqueous As(V)	$4\,HAsO_4^{2-} + C_2H_4O_2 + 6\,H^+ \rightarrow 4\,H_3AsO_3 + 2\,HCO_3^-$	$R_{resp}^{11} = k_{resp}^{HAsO_4^{2-}}\cdot\left[CH_3COO^-\right]\cdot\left(\frac{[HAsO_4^{2-}]}{K_{m\,(resp)}^{HAsO_4^{2-}}+\left[HAsO_4^{2-}\right]}\right)\left(\frac{K_{in}^{O_2}}{K_{in}^{O_2}+\left[O_2\right]}\right)$	11
Equilibrium adsorption of As(III)	$H_3AsO_3 + 2{\equiv}SOH \rightleftarrows {\equiv}S_2HAsO_3 + 2\,H_2O$	$logK_{sorp}^{H_3AsO_3}$	12
Kinetic sorption of As(III)	$H_3AsO_3 + 2{\equiv}SOH \rightleftarrows {\equiv}S_2HAsO_3 + 2\,H_2O$	$R_f^{13} = k_f^{H_3AsO_3}\cdot[H_3AsO_3] R_b^{14} = k_b^{H_3AsO_3}\cdot{\equiv}S_2HAsO_3$	13
			14
		$R_i^{15} = k_i^{H_3AsO_3}\cdot{\equiv}S_2HAsO_3$	15
Oxidative biomethylation of As(III)	$CH_4 + H_3AsO_3 \rightarrow CH_3As^VO(OH)_2 + 2\,H^+ + 2\,\bar{e}$	$R_{methyl}^{16} = r_{max}^{H_3AsO_3}\cdot\left(\frac{[H_3AsO_3]}{K_m^{H_3AsO_3}+[H_3AsO_3]}\right)\left(\frac{K_{in}^{O_2}}{K_{in}^{O_2}+[O_2]}\right)$	16
Antimony			
Equilibrium adsorption of Sb(V)	$Sb(OH)_6^- + 2\,{\equiv}SOH \rightleftarrows ({\equiv}SO)_2Sb(OH)_4^- + 2\,H_2O$	$logK_{sorp}^{Sb(OH)_6^-}$	17
Kinetic sorption of Sb(V)	$Sb(OH)_6^- + 2\,{\equiv}SOH \rightleftarrows ({\equiv}SO)_2Sb(OH)_4^- + 2\,H_2O$	$R_f^{18} = k_f^{Sb(OH)_6^-}\cdot[Sb(OH)_6^-]$	18
		$R_b^{19} = k_b^{Sb(OH)_6^-}\cdot({\equiv}SO)_2Sb(OH)_4^-$	19
		$R_i^{20} = k_i^{Sb(OH)_6^-}\cdot({\equiv}SO)_2Sb(OH)_4^-$	20
Detoxification of surface-bound Sb	$({\equiv}SO)_2Sb(OH)_4^- + 3\,H^+ + 2\,\bar{e} \rightarrow Sb(OH)_3 + 3H_2O$	$R_{detox}^{21} = r_{max}^{Sb(OH)_6^-}\cdot\left(\frac{({\equiv}SO)_2Sb(OH)_4^-}{K_{m\,(detox)}^{Sb(OH)_6^-}+({\equiv}SO)_2Sb(OH)_4^-}\right)$	21

Description	Reaction	Kinetic or equilibrium formulation	R#

(*continued on next page*)

Table 2 (*continued*)

Description	Reaction	Kinetic or equilibrium formulation	R#
Respiration of aqueous As(V)	4 $HAsO_4^{2-}$ + $C_2H_4O_2$ + 6 H^+ → 4 H_3AsO_3 + 2 HCO_3^-		$R_{resp}^{11} = k_{resp}^{HAsO_4^{2-}} \cdot \left[CH_3COO^-\right] \cdot \left(\frac{[HAsO_4^{2-}]}{K_{m\,(resp)}^{HAsO_4^{2-}} + \left[HAsO_4^{2-}\right]}\right)\left(\frac{K_{in}^{O_2}}{K_{in}^{O_2} + \left[O_2\right]}\right)$
11			
Precipitation of Sb (III)	Sb_2O_3 (c) + 3 H_2O ⇄ 2 $Sb(OH)_3$ (aq)	$logK_{sp}^{Sb_2O_3}$	23
Chromium			
Equilibrium adsorption of Cr(VI)	CrO_4^{2-} + ≡SOH + H^+ ⇄ $\equiv SOH_2{}^+CrO_4^{2-}$	$logK_{sorp}^{CrO_4^{2-}}$	24
Kinetic sorption of Cr(VI)	CrO_4^{2-} + ≡SOH + H^+ ⇄ $\equiv SOH_2{}^+CrO_4^{2-}$	$R_f^{25} = k_f^{CrO_4^{2-}} \cdot [CrO_4^{2-}]$	25
		$R_b^{26} = k_b^{CrO_4^{2-}} \cdot \equiv SOH_2^+CrO_4^{2-}$	26
		$R_i^{27} = k_i^{CrO_4^{2-}} \cdot \equiv SOH_2^+CrO_4^{2-}$	27
Abiotic reduction of surface-bound Cr(VI)	$\equiv SOH_2{}^+CrO_4^{2-}$ + 5 H^+ + 3 $\bar{e}$ → $Cr(OH)_{3(s)}$ + H_2O	$R_{ab}^{28} = k_{ab}^{CrO_4^{2-}} \cdot \equiv SOH_2^+CrO_4^{2-}$	28
Detoxification of aqueous Cr (VI)	CrO_4^{2-} + 5 H^+ + 3 $\bar{e}$ → $Cr(OH)_{3(s)}$ + H_2O		$R_{detox}^{29} = r_{max}^{CrO_4^{2-}} \cdot \left(\frac{[CrO_4^{2-}]}{K_{m\,(detox)}^{CrO_4^{2-}} + \left[CrO_4^{2-}\right]}\right)$
29			

Description	Reaction	Kinetic or equilibrium formulation	R#
Respiration of aqueous Cr (VI)	8 CrO_4^{2-} + 3 CH_3COO^- + 13 H^+ + +4 H_2O → 8 Cr $(OH)_3$ + 6 HCO_3^-		$R_{resp}^{30} = k_{resp}^{CrO_4^{2-}} \cdot \left[CH_3COO^-\right] \cdot \left(\frac{[CrO_4^{2-}]}{K_{m\,(resp)}^{CrO_4^{2-}} + \left[CrO_4^{2-}\right]}\right)\left(\frac{K_{in}^{O_2}}{K_{in}^{O_2} + \left[O_2\right]}\right)$
30			
Precipitation of Cr (III)	$Cr(OH)_{3(s)}$ + H+ ⇄ $Cr(OH)_2{}^+$ + H_2O	$logK_{sp}^{Cr(OH)_3}$	31
Nitrogen			
Respiration of N (V)	2 NO_3^- + CH_2O → 2 NO_2^- + CO_2 + H_2O		$R_{resp}^{32} = k^{NO_3^-} \cdot [CH_2O] \cdot \left(\frac{[NO_3^-]}{K_m^{NO_3^-} + [NO_3^-]}\right)\left(\frac{K_{in}^{O_2}}{K_{in}^{O_2} + [O_2]}\right)\left(\frac{K_{in}^{CrO_4^{2-}}}{K_{in}^{CrO_4^{2-}} + [CrO_4^{2-}]}\right)$
32			
Respiration of N (III)	4 NO_2^- + 3 CH_2O + 4 H^+ → 2 N_2 + 3 CO_2 + 5 H_2O		$R_{resp}^{33} = k^{NO_2^-} \cdot [CH_2O] \cdot \left(\frac{[NO_2^-]}{K_m^{NO_2^-} + [NO_2^-]}\right)\left(\frac{K_{in}^{O_2}}{K_{in}^{O_2} + [O_2]}\right)\left(\frac{K_{in}^{CrO_4^{2-}}}{K_{in}^{CrO_4^{2-}} + [CrO_4^{2-}]}\right)$
33			

Comments:
- ≡SOH: a generic sorption site, which can be protonated or non-protonated and may involve one, two or three surface oxygens.
- CH_2O: dissolved organic carbon released by the argillaceous matrix.
- Detoxification: microbial reduction of As, Sb and Cr, which is not coupled to the oxidation of an external electron donor.
- Respiration: microbial reduction of As, Sb and Cr, which is coupled to the oxidation of ethanol or acetate.

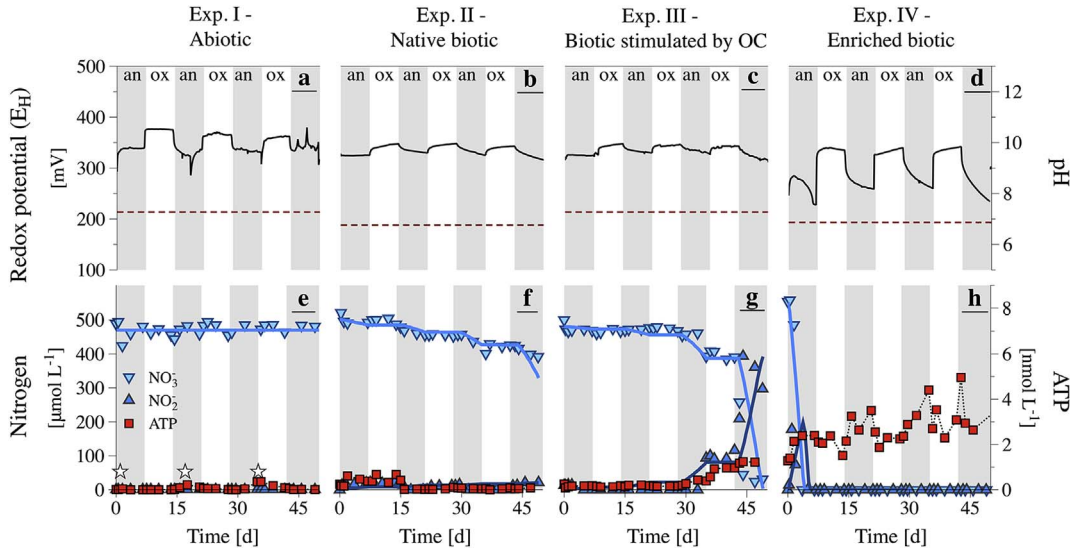

Fig. 1. Time series of measured redox potential (E_H) (line) and pH (dashed line) values (a–d), nitrate (NO_3^-) (down-pointing triangle), nitrite (NO_2^-) (up-pointing triangle), and ATP concentrations (squares connected by dashed line) (e–h). Modelled concentrations of NO_3^- and NO_2^- are indicated by solid lines. Addition of microbial inhibitors is indicated by stars (e), whereas shaded and white areas indicate anoxic (CO_2 + N_2) and oxic (O_2 + CO_2 + N_2) periods, respectively.

model, that for Exp. IV, was obtained by adding rates accounting for microbial respiration to the model for Exp. II-III. The entire reaction network used in the biogeochemical models is given in Table 2. The assumptions and kinetic formulations are explained in the discussion section where we refer to the reaction numbers indicated in the table.

An optimization algorithm was implemented in Python. The scipy.optimize package (Jones et al., 2001) was used to minimize root-mean-square errors (RMSE) and select the subset of parameters yielding the best fit between model and data. A global sensitivity analysis was performed to ascertain how the predictive models depend on parameter values via a Fourier Amplitude Sensitivity Test (FAST) (Saltelli et al., 1999) by using the open source Python library SALib (Herman and Usher, 2017). The sensitivity of the predicted aqueous concentrations to parameter values was analysed by varying parameters one at a time ("First") and by accounting for the sum of the interaction effects ("Total"). The respective sensitivity indices were estimated by running the models with a distribution of parameters within a range spanning four orders of magnitude.

3. Results

3.1. Argillaceous matrix characterization

The mineralogical composition of the Tégulines argillaceous geomaterial (Table A.1) was dominated by clay minerals (muscovite, smectite, kaolinite, biotite, chlorite, microcline) (56%), quartz (29%), calcite (12%), and minor amounts (< 2%) of gypsum, pyrite, and anatase. The material was depleted in reducible Fe plus Mn minerals and reactive Al phases (CDB extract), which together comprised less than 0.2% dry weight (d.w.) (Table A.2). The major cations indicated typical clay composition (Table A.2): SiO_2 (56%), Al_2O_3 (14%), CaO (8%), Fe_2O_3 (5%), K_2O (2%), MgO (1%), TiO_2 (0.7%), Na_2O (0.2%), P_2O_5 (0.1%). The residual dry weight (11%) was lost on ignition.

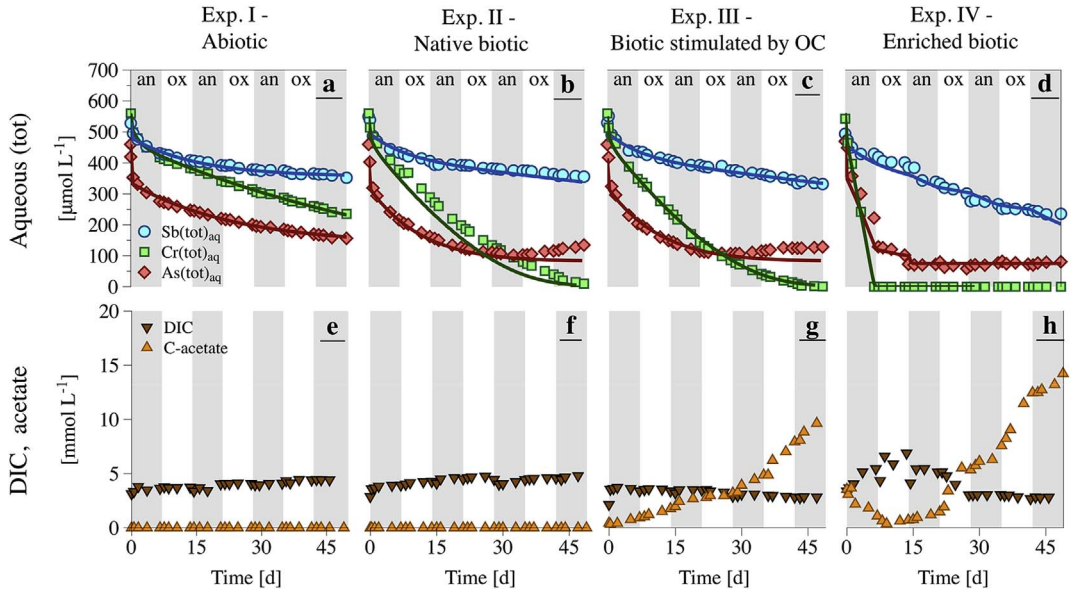

Fig. 2. Time series of modelled (line) and measured [As] (diamond), [Sb] (circle), and [Cr] (square) aqueous concentrations, (a–d); measured concentrations of dissolved inorganic carbon (DIC) (down-pointing triangle) and carbon in the form of acetate (up-pointing triangle) (e–h).

3.2. Redox potential (E_H), pH and microbial activity

The imposed cycles of oxic and anoxic conditions resulted in reproducible fluctuations of E_H values, which remained above +200 mV throughout all experiments (Fig. 1: a-d). The E_H of the sterilized argillaceous suspension (Exp. I) oscillated between +368 ± 8 and +338 ± 10 mV under oxic and anoxic conditions, respectively. The E_H profiles were similar in Exp. II and Exp. III with average oxic and anoxic values of +345 ± 5 and +338 ± 10 mV, respectively. The corresponding E_H values in Exp. IV were +342 ± 4 (oxic) and +245 ± 15 (anoxic) mV. The pH remained stable at near-neutral values (7.1 ± 0.1) throughout all experiments (Fig. 1: a-d).

In Exp. I, the NO_3^- concentration remained constant at its initial level (488 ± 11 μM) and no nitrite (NO_2^-) was detected in solution; ATP concentrations were low or undetectable throughout the experiment (Fig. 1: e). When trace concentrations of ATP were measured (< 0.3 nM) on days 17 and 35, additional injections of microbial inhibitors were performed. In Exp. II, NO_3^- decreased during anoxic periods reaching 390 μM at the end of the experiment (initial concentration was 520 μM); up to 20 μM of NO_2^- was measured, although it did not persist in solution (Fig. 1: f). At the beginning of Exp. II, ATP was 0.3 nM; it increased thereafter, stabilizing at 0.7 nM during the first 19 days, then decreasing to 0.1 nM and remaining stable at this level (Fig. 1: f).

In Exp. III, with ethanol additions, NO_3^- concentrations decreased at a similar rate as in Exp. II over the first 30 days while ATP remained stable at 0.20 ± 5 nM. By the end of the 3rd anoxic period, NO_3^- reduction accelerated and NO_2^- increased up to 395 μM during the 4th anoxic period, coincident with an increase of ATP to 1.24 nM (Fig. 1: g). During the oxic period between the 3rd and 4th anoxic periods, the concentrations of NO_3^-, NO_2^-, and ATP remained constant. In Exp. IV, the addition of soil inoculum resulted in the highest initial ATP concentration of 1.3 nM, and the fastest NO_3^- reduction to NO_2^-, followed by a complete removal of NO_3^- and NO_2^- from solution during the 1st anoxic period. In the absence of NO_3^- and NO_2^-, ATP concentrations continued to gradually increase, reaching 5.0 nM by the 4th anoxic period (Fig. 1: h). ATP concentrations decreased during oxic periods (higher E_H) and increased during anoxic periods (lower E_H) resulting in a statistically significant negative correlation between ATP and E_H ($r = -0.22$, $p < .005$).

3.3. Solution chemistry

During the pre-equilibration period, 0.41 ± 0.04 mM (0.1 mg g^{-1} solid) of DOC was released from the argillaceous matrix into solution in all four experiments. The low absorbance ($UVA_{254} = 0.2$, SUVA = 0.04) suggested a primarily aliphatic structure. In the absence of ethanol additions, DOC accumulated in solution to 47.8 and 42.7 mM in Exp. I and Exp. II, respectively (Fig. B.2). The constant rate of DOC accumulation significantly correlated with that of Cl^- ($r = 0.99$, $p < .005$) indicating a common source: leakage from the pH and E_H electrodes (Fig. B.1). Further supporting information can be found in Appendix B.

During experiments with ethanol additions we observed a step-wise increase in total DOC concentration up to 54.3 mM (Exp. III) and 56.5 mM (Exp. IV), of which, acetate accounted for 5 and 7.5 mM, respectively (Fig. 2: g-h). In Exp. IV, 1.8 mM acetate was initially present due to the addition of the soil inoculum. It became depleted to 0.25 mM during the first 15 days and accumulated in solution up to 7 mM during the rest of the experiment. The decrease in acetate concentration was coincident with increased DIC concentration from 4 to 7 mM by day 15 (Fig. 2: h). The concentration of DIC was relatively stable (4.05 ± 0.5 mM) in all other experiments (Fig. 2: e-g).

Calcite dissolution (SI = −0.33 at 25 °C, $pCO_2 = 10^{-2}$ atm) likely controlled the increase of [Ca] from 3 to 6 mM in all experiments. Total [Fe] was generally ~2 μM (Fig. B.1: a); [Mn] was around 0.5–0.9 μM initially and remained constant in Exp. I – II, while it increased to 2.7 and 5.7 μM by the end of Exp. III and Exp. IV, respectively (Fig. B.1: b); [S] remained unchanged with time and was always present as ~6 mM sulfate (SO_4^{2-}) (Fig. B.1: c).

3.4. Contaminant behaviour

Under abiotic conditions in Exp. I, contaminant behaviour was not affected by the oscillations between oxic and anoxic cycles. Total aqueous [As] continuously decreased from 460 to 159 μM, [Sb] from 528 to 352 μM, and [Cr] from 560 to 235 μM (Fig. 2: a). Over the course of the experiment, twice as much As and Cr were removed from solution compared to Sb. Aqueous contaminant speciation analyses indicated that all contaminants remained in their initial oxidized states (Fig. B.3). Solid-phase As and Sb speciation analyses suggested that these elements were sequestered by the argillaceous matrix in their oxidized forms. In contrast, 90% of Cr was immobilized in the solid phase as reduced Cr(III) (Fig. A.2).

In Exp. II, [As] steadily decreased from 460 to 105 μM during the first 30 days and increased only slightly afterwards to 135 μM (Fig. 2: b). The decrease of [As] was coincident with removal of As(V) from solution and the appearance of As(III) (Fig. B.3: a). Selective extraction results suggested that 83% of sequestered As in the solid-phase was present as As(V) and 17% as As(III) by day 49 (Fig. A.2: a). Slightly more aqueous Sb was removed in Exp. II than in Exp. I. This is consistent with greater solid phase accumulation of Sb in Exp. II, of which 20% occurred as Sb(III) (Fig. A.2: b). Aqueous [Cr] decreased below the detection limit (0.05 μM) by the last day of the experiment with concurrent accumulation in the solid phase as Cr(III) (> 98%) (Fig. A.2: c).

In Exp. III, aqueous As, Sb, and Cr were sequestered as in Exp. II, although at slightly faster rates. [As] decreased from 460 to 110 μM over 26 days (Fig. 2: c), concomitant with complete reduction of aqueous As(V) to As(III) (Fig. B.3: a), and As(III) accumulation in the solid-phase by the end of the experiment. Antimony, again, was sequestered to a lesser extent than the other contaminants and remained in solution entirely as Sb(V), though, about 15% of solid-phase Sb was found to be Sb(III). [Cr] behaved as in Exp. II, although depletion from solution was faster, which appeared to trigger the onset of NO_3^- reduction.

In Exp. IV, the contaminants were sequestered to the greatest extent. In this experiment, the removal rates were affected by the oscillating oxic and anoxic conditions (Fig. 2: d). Decreases in [As] were only observed under anoxic conditions; after day 15 all remaining aqueous As was under the form of As(III). Complete As(V) removal from solution appeared to enhance Sb(V) removal: after day 15, [Sb] decreased at twice the initial rate. By the end of the experiment, only Sb(V) was detected in the aqueous phase (Fig. B.3: b), while oxidized and reduced Sb were detected in a 4:1 ratio in the solid-phase (Fig. A.2). Chromium (VI) was completely reduced and removed from solution to below detectable concentrations (< 0.05 μM) during the first anoxic period.

Comparison of contaminant removal from the aqueous phase with accumulation in the solid phase at the end of the experiments showed good mass balances (Fig. A.1). The only exception was Sb removal from solution in Exp. IV, which indicated a 18% Sb deficit from the solid-phase. Overall, sequestered contaminants were predominantly present as As(V), Sb(V), and Cr(III) comprising > 75% of their total solid-phase accumulation by day 49 in Exp. IV (Fig. 5).

4. Discussion

4.1. Abiotic sequestration of As, Sb, Cr in Exp. I

4.1.1. Distribution coefficients (Kd)

We used the model derived for Exp. I to extrapolate the aqueous contaminant concentrations in equilibrium with the argillaceous mineral matrix beyond the experimental time period. The modelling results suggest that equilibrium partitioning would be reached after 72

Table 3
Forward (k_f), backward (k_b) and irreversible (k_i) rate constants, plus the equilibrium sorption constant (log K) used in the multi-reaction models. Estimated distribution (or partition) coefficients (Kd) of As(V), As(III), Sb(V), and Cr(V) for sorption to the Tégulines matrix in Exp. I.

Sorbate	Kd (L kg^{-1})	k_f (h^{-1})	k_b (h^{-1})	k_i (h^{-1})	Log K	RMSE
As(V)	46.7	3.0×10^{-3}	5.8×10^{-3}	2.3×10^{-3}	−0.54	1.55
As(III)	–	1.7×10^{-5}	4.8×10^{-2}	2.7×10^{-3}	−0.38	–
Sb(V)	9.8	1.1×10^{-3}	4.2×10^{-3}	6.7×10^{-4}	−1.07	3.01
Cr(VI)	11108	4.0×10^{-3}	3.8×10^{-2}	0.0	−1.03	6.54

days for Sb(V), 113 days for As(V), and 400 days for Cr(VI). The predicted contaminant equilibrium concentrations were used to calculate distribution coefficient (Kd) values (Table 3) specific to the experimental conditions: suspension density (50 g L^{-1}), total contaminant concentrations (~500 µM), pH (7.1 ± 0.1), ionic strength (0.05 M), and temperature (25 °C).

Derived Kd values for As and Sb are lower than those reported in the literature for pure clay phases. For example, at near-neutral pH, Kd values of Sb(V) in pure kaolinite suspensions vary from 73 to 115 L kg^{-1} according to the experimental data of Rakshit et al. (2015). This Kd range can be reconciled with the Kd value (9.8 L kg^{-1}) calculated for Sb(V) in the present study when taking into account that kaolinite represents 11% d.w. of the argillaceous matrix. Similarly, the Kd value of As(V) in Exp. I (46.7 L kg^{-1}) is consistent with the Kd for pure muscovite at neutral pH (282–416 L kg^{-1}) (Chakraborty et al., 2007), given the 15% d.w. content of muscovite in the argillaceous matrix. The Kd value of Cr is much higher than those of As and Sb because of the inferred reductive precipitation mechanism, which completely removes Cr from solution.

4.1.2. Arsenic abiotic sequestration

Similar to As(V) sequestration by pure mineral phases (Couture et al., 2013) and natural soils (Zhang and Selim, 2005), As(V) adsorption to the Tégulines matrix in Exp. I is best described by a two-phase process with an initial rapid (equilibrium) uptake followed by a slow kinetic immobilization (Fig. 3: a). The model yields an apparent equilibrium sorption constant log K = −0.54 (Table 3), which describes the instantaneous removal of 30% of the aqueous As(V), likely via the formation of outer-sphere complexes. The reversible kinetic uptake, presumably through the formation of inner-sphere complexes, is represented by the adsorption (k_f) and desorption (k_b) rate constants. The k_f and k_b values for As(V) in this study are up to 3 orders of magnitude lower than those estimated for As(V) sorption on Fe-bearing minerals (2-line ferrihydrite, goethite, amorphous mackinawite, pyrite; Couture et al., 2013) and natural soils containing 5.7 ± 2 mg g^{-1} of amorphous Fe_2O_3 (Oliver loam, Sharkey clay, Windsor sand; Zhang and Selim, 2005).

Clays offer a variety of sites suitable for As(V) sorption on (1) broken clay edges via surface ligand exchange (Charlet et al., 2012; Lin and Puls, 2000; Wilson et al., 2010), (2) negatively charged clay surfaces (e.g., kaolinite) at neutral pH via cation (e.g., Ca^{2+}) bridging (Sharma and Kappler, 2011), and (3) hydroxide interlayers in the clay structure of chlorite (Lin and Puls, 2000). All of these mechanisms are likely to play a role in our experiments, given the presence of kaolinite (11% d.w.) and chlorite (3.9% d.w.), pH of 7.2 and high [Ca] (4 mM). Sorption onto calcite (12% d.w.) at ambient carbon dioxide pressure ($pCO_2 = 10^{-3.5}$ atm) would require a higher pH (> 8.3) (Sø et al., 2008).

Slow As(V) removal, which is implemented in the model as an irreversible kinetic reaction, most probably represents intra-/inter-

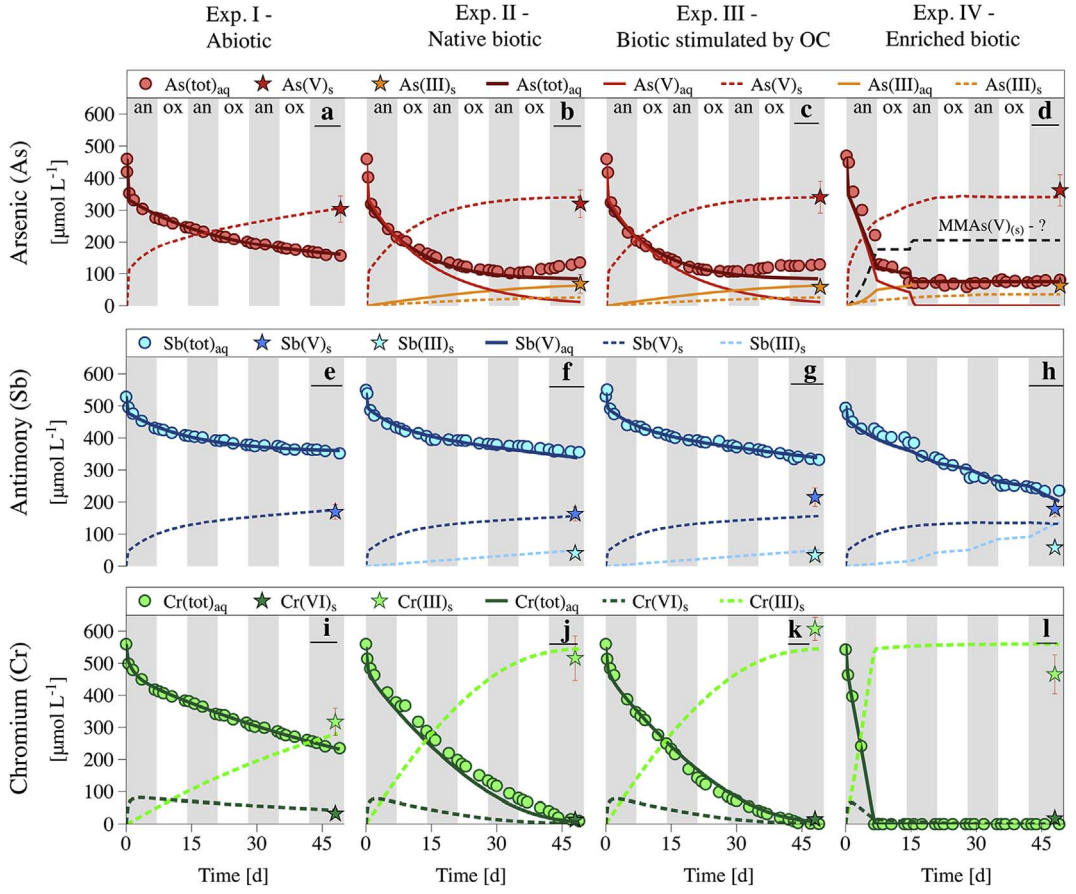

Fig. 3. Time series of measured total aqueous concentrations (circle) and solid speciation (star) of As (a–d), Sb (e–h), and Cr (i–l). Reaction formulations and parameters used in the models to predict aqueous (solid line) and solid (dashed line) speciation are given in Table 2 and described in Appendix D.

particle diffusion (Zhang and Stanforth, 2005) or the formation of surface precipitates (Gallegos et al., 2007), such as Ca-arsenate phases (Bothe and Brown, 1999; Raposo et al., 2004). Based on the initial [As] concentration in Exp. I, the experimental solution is oversaturated with respect to several Ca-As phases: $Ca_3(AsO_4)_2(H_2O)_4$ (SI = 6.1) and $Ca_3(AsO_4)_2$ (SI = 6.3). Hence, thermodynamically, the formation of such precipitates is possible, although likely rate-limited.

4.1.3. Antimony abiotic sequestration

Modelling results suggest that sequestration of Sb(V) (Fig. 3: e) is mainly kinetically-controlled with the initial equilibrium uptake accounting for only 5% of total Sb sequestration (log K = −1.07) (Table 3). This is consistent with results suggesting low Sb(V) sorption on clay minerals (i.e., kaolinite) at neutral pH (Rakshit et al., 2015). Estimated rate constants of Sb(V) adsorption and desorption are on the same order of magnitude as those of As(V). The fact that the Sb(V) desorption rate constant (k_b) is higher than that of sorption (k_f), together with the very low irreversible sequestration rate constant (k_i), suggests that Sb(V) uptake is mostly reversible, as previously observed (Johnson et al., 2005; Xi et al., 2010), although precipitation of $Ca[Sb(OH)_6]_2$ (Johnson et al., 2005) is thermodynamically possible (SI = 3.33) in Exp. I.

4.1.4. Chromium abiotic sequestration

In contrast to As(V) and Sb(V), which remained oxidized under abiotic conditions, Cr(VI) was reduced and accumulated in the solid phase as Cr(III). Chromium is a strong oxidant which can be reduced at surface sites of Fe(II)-bearing clay minerals and pyrite (Chon et al., 2006) to form $Cr(OH)_{3(am)}$, $Cr(OH)_3{\cdot}H_2O_{(cr)}$, Cr_2O_3, or $(Cr,Fe)(OH)_3$ (Nriagu et al., 1993), even in the presence of O_2 (Rai et al., 1989). The continuous decrease of [Cr] during oxic and anoxic periods (Fig. 3: i) corroborates that abiotic Cr reduction is not inhibited by O_2. Moreover, Cr(VI) can be reduced by DOC (Jamieson-Hanes et al., 2012) released from the argillaceous matrix itself.

The measured speciation of solid-phase Cr implies a two-step uptake mechanism with adsorption of Cr(VI) followed by its abiotic reduction leading to Cr sequestration as $Cr(OH)_3$ (SI = 1.18) (Fig. 3: i). The modelled mechanism is consistent with the XANES results of Jamieson-Hanes et al. (2012) demonstrating that Cr reduction occurs at particle surfaces rather than in solution. Assuming constant pH, we introduce a first-order kinetic reduction rate of adsorbed Cr(VI) (Table 2, R^{28}). The rate constant derived from fitting the data (3.9×10^{-3} h^{-1}; Table D.2) is close to that reported for soil (6.9×10^{-3} h^{-1}; Matern and Mansfeldt, 2016). Overall, the model suggests weak Cr(VI) sorption on the argillaceous matrix consistent with previous reports for kaolinite, montmorillonite, and illite (Lan et al., 2008). Abiotic sequestration of Cr(VI) is thus interpreted as mainly resulting from reductive precipitation, which sequesters ~50% of aqueous Cr with the rest (~8%) being removed via surface adsorption (Fig. 5).

4.2. Microbial effects on the mobility of As, Sb, Cr in Exp. II, III, IV

4.2.1. Microbial activity

The observed temporal trends of NO_3^- and ATP concentrations indicate that in Exp. II – III microorganisms were present and active in the bioreactors, while they were inactive in the sterilized suspension of Exp. I (Fig. 1: e-h). Nitrate reduction is associated with energy production (Konhauser, 2007) and a corresponding ATP increase is observed in Exp. III (Fig. 1: k): ATP concentrations and NO_3^- (Exp. III – IV) reduction rates are significantly correlated (r = 0.99, p < .001).

The electron donor for NO_3^- reduction is likely naturally present in the argillaceous matrix. Ethanol is an unlikely reductant, as the NO_3^- reduction rate did not respond to the ethanol additions during the 1st, 2nd, and 3rd anoxic periods of Exp. III. Theoretically, DOC released by the argillaceous matrix during the pre-equilibration period (0.1 mg g^{-1}) may attenuate about 12 µmol g^{-1} of NO_3^-, assuming a zero oxidation state of DOC. Moreover, pyrite within the argillaceous matrix may attenuate up to 417 µmol g^{-1} of NO_3^-. Even though nitrate reduction coupled to organic carbon and pyrite oxidation are both widespread processes under biotic conditions (Bosch et al., 2012), the higher energy yield of NO_3^- reduction with organic matter should favor this reaction pathway over anaerobic pyrite oxidation (Appelo and Postma, 2005). Complete reduction of NO_3^- by pyrite would also lead to an increase in SO_4^{2-} and Fe by 350 and 175 µM, respectively, which was not observed (Fig. B.1: c). We therefore model nitrate consumption as a heterotrophic denitrification pathway with complete NO_3^- turnover via NO_2^- to $N_{2(g)}$ coupled to the oxidation of DOC (Table 2, $R^{32,33}$) (Rivett et al., 2008).

4.2.2. Fate of As in the presence of microorganisms

The occurrence of As(V) reduction in Exp. II – III, which did not occur in Exp. I (Fig. A.2, Fig. B.3), suggests a microbially mediated reaction. Reduction rates are similar regardless of the addition of ethanol, again implying that this carbon source is not used as a primary electron donor for As reduction. Microbial As reduction can either proceed via enzymatic (respiration and detoxification) or non-enzymatic (oxidation of microbially produced glutathione) pathways (Scott et al., 1993). Given that our experimental [As] values exceed the threshold of 100 µM As for expression of detoxification genes by bacteria *Shewanella* sp. (Saltikov et al., 2005) by 4-fold, reduction by detoxification is a plausible pathway.

The detoxification mechanism is also supported by the lack of ATP increase throughout Exp. II – III (Fig. 1: f-g), suggesting that As reduction is not an energy gaining process for the native microbial community (Lloyd and Oremland, 2006; Oremland et al., 2009; Plant et al., 2005). In agreement with the observations of Saltikov et al. (2005) who reported aerobic As(V) detoxification by *Shewanella* sp. ANA-3, As reduction is not inhibited by the presence of O_2 in our study (Fig. 3: b-c). Moreover, other terminal electron acceptors (TEAs) of higher redox potential (Table 4) did not inhibit the reduction of As(V) to As(III) (Fig. B.3), which occurred simultaneously with CrO_4^{2-} and NO_3^- reduction. The often-hypothesized thermodynamic cascade of TEA utilization is therefore not observed. Finally, the fact that ethanol additions did not increase the As reduction rate supports detoxification over respiration as an As-reduction mechanism. In the absence of a suitable external electron donor, possible electron donors for detoxification are endogenous reservoirs (e.g., DNA and proteins) mediated by intracellular reductants (e.g., NADH, NADPH, ascorbate, glutaredoxin, glutathione; Silver and Phung, 2005).

To account for both mineralogical and microbial controls on As sequestration in Exp. II – III, Monod-type kinetic expressions are added to the multi-reaction model of Exp. I. We assume that the rate of

Table 4
Thermodynamic sequence based on the redox potentials (E_H) of half reduction reactions at the experimental pH (6.9), temperature (25 °C), and activities of reduced and oxidized species at the beginning of Exp. IV. The thermodynamic order of As and Sb reduction differs depending on pH ($E_H{}^{\circ\prime}$ and $E_H{}^{\circ}$) and products of Sb reduction. The observed experimental sequence of Sb reduction followed by As reduction, suggests Sb reduction to $Sb_2O_{3(s)}$, rather than to $Sb(OH)_3$. Calculations are based on the thermodynamic values given in Bard et al. (1985); Filella and May (2003); Nordstrom et al. (2014); Tratnyek and Macalady (2000); Zotov et al (2003).

Half-reduction reactions	E_H [mV] pH 6.9	$E_H{}^{\circ\prime}$ [mV] pH 7	$E_H{}^{\circ}$ [mV] pH 0
$O_2 + 4\,H^+ + 4\,\bar{e} \rightarrow 2\,H_2O$	815	816	1230
$CrO_4^{2-} + 5\,H^+ + 3\,\bar{e} \rightarrow Cr(OH)_3 + H_2O$	524	579	1270
$NO_3^- + 2\,H^+ + 2\,\bar{e} \rightarrow NO_2^- + H_2O$	316	426	840
$Sb(OH)_6^- + 3\,H^+ + 2\,\bar{e} \rightarrow Sb(OH)_3 + 3\,H_2O$	188	91	712
$HAsO_4^{2-} + 4\,H^+ + 2\,\bar{e} \rightarrow H_3AsO_3 + H_2O$	160	18	846
$2\,Sb(OH)_6^- + 6\,H^+ + 4\,\bar{e} \rightarrow Sb_2O_{3(s)} + 9\,H_2O$	130	218	839
$CO_2 + 12\,H^+ + 12\,\bar{e} \rightarrow C_2H_5OH$ (ethanol) $+ 3\,H_2O$	−795	−356	90

detoxification is independent of the DOC concentration and not inhibited by O_2 (Table 2, R^{10}). Modelling results indicate that the persistence of As(III) in solution is consistent with its low sorption affinity to clay minerals (Table 3; Lin and Puls, 2000) and the under-saturation of the solution with respect to $CaHAsO_3$ (SI = −0.38). We note that the model fails to capture the observed slight increase of aqueous [As] between day ~30 and the end of Exp. II – III (Fig. 3: b-c). Late As remobilization could reflect the re-equilibration of surface-bound As (III) with the solution under evolving geochemical conditions. Alternatively, the release of As(III) in solution could be a result of late reduction of surface-bound and, thus, less bioavailable As(V) (Ghorbanzadeh et al., 2015).

In Exp. IV, the inoculation of soil microorganisms resulted in the inhibition of As(V) reduction by O_2 during the first oxic period (Fig. 3: d). Furthermore, As(V) reduction was associated with a 1:1 conversion of carbon in a form of acetate to DIC (Fig. 2: h), consistent with acetate oxidation to bicarbonate. Because acetate may provide electrons for microbial As reduction (Lloyd and Oremland, 2006; Oremland et al., 2009), it can enable As respiration (Gorny et al., 2015). An increase in ATP concentration, expected for enhanced microbial respiration (Oremland, 2005), is also observed (Fig. 1: h).

In the model, As(V) respiration is simulated by a rate expression that accounts for inhibition by O_2 and depends on the availability of organic carbon (acetate) (Table 2, R^{11}). Initial model runs, however, overestimated [As] remaining in solution and underestimated As(V) accumulation in the solid phase (Fig. D.3: b). A potential mechanism, accounting for the missing As(V), is sorption of non-volatile mono-methyl As (MMAs(V); Lafferty and Loeppert, 2005) formed via oxidative biomethylation of As(III) (Mestrot et al., 2013). This mechanism is speculative due to the lack of direct experimental confirmation, but weakly supported by its inhibition at the initiation of Sb(V) reduction. The inhibition of As biomethylation in the presence of Sb(III) has been demonstrated by Andrewes et al. (2000). We therefore added the oxidative biomethylation of As(III) in the model (Table 2, R^{16}). The modelling exercise reveals that ~46% of As(III) could be immobilized via sorption of freshly formed methylated As(V) (Fig. 3: d). The overall aqueous As(V) concentration predicted by the model is most sensitive to the rates of abiotic adsorption ($k_f^{HAsO_4^{2-}}$) and microbial respiration ($k_{resp}^{HAsO_4^{2-}}$) (Fig. D.4) suggesting that both sorption and reduction mechanisms play significant roles in As(V) sequestration (Fig. 5).

4.2.3. Fate of Sb in the presence of microorganisms

Similar to As, reduction of Sb(V) to Sb(III) is mediated by native microorganisms and suggestive of a detoxification mechanism in Exp. II – III (Fig. 3: f-g). Based on the saturation index, precipitation of Sb(III) in the form of $Sb_2O_{3(s)}$ (SI = 0.69) is thermodynamically possible, consistent with microbial Sb(V) reduction (Abin and Hollibaugh, 2014). Fast reductive precipitation of Sb agrees with the absence of aqueous Sb (III) and the co-existence of Sb(V) with As(III) in the experimental solutions of Exp. II and III, as previously demonstrated in other studies (Casiot et al., 2007; Fawcett et al., 2015; Mitsunobu et al., 2006). The model fit to the experimental data requires a two-step process: sorption of Sb(V) followed by its reduction at the mineral surfaces, presumably via a detoxification pathway (Table 2, R^{21}). This would suggest that the microorganisms capable of Sb detoxification are surface-associated rather than planktonic. To our knowledge, such a mechanism has not yet been described in the literature.

In Exp. IV, after complete As(V) removal by day 15, the removal rate of aqueous Sb increased, but only during the anoxic periods (Fig. 3: h). Recent studies have demonstrated that under anoxic conditions, Sb(V) can act as a TEA for microbial respiration (Abin and Hollibaugh, 2014), but also that Sb(V) respiration is inhibited by the presence of aqueous As(V) (Fawcett et al., 2015; Kulp et al., 2014; Mitsunobu et al., 2006). Thus, Sb(V) respiration could explain the increase of ATP observed in Exp. IV following the complete reduction of alternative TEAs (CrO_4^{2-}, NO_3^-, and $HAsO_4^{2-}$) (Fig. 1: h).

The observed sequence of As(V) reduction prior to Sb(V) reduction agrees with the thermodynamic sequence based on the calculated E_H values of the TEA reduction reactions (Table 4). Under the experimental conditions (pH ~7, 25 °C), As(V) is expected to suppress Sb(V) reduction to solid-phase $Sb_2O_{3(s)}$, but not to aqueous $Sb(OH)_{3(aq)}$. Microbial reductive precipitation of $Sb_2O_{3(s)}$, coupled to the oxidation of lactate to acetate, has been reported by Abin and Hollibaugh (2014). Likewise, in Exp. IV, a gradual accumulation of acetate in solution after day 15 (Fig. 2: h) suggests that Sb reduction is coupled to the oxidation of ethanol to acetate. Although a large number of studies have previously compared the biogeochemical properties of Sb and As (e.g., Dovick et al., 2016; Willis et al., 2011; Wilson et al., 2010), the incomplete oxidation of organic carbon by Sb(V), in contrast to complete mineralization to DIC by As(V), has not previously been highlighted.

Inclusion of Sb(V) reduction in the model, via a respiration mechanism which is inhibited by dissolved O_2 and aqueous As(V) (Table 2, R^{22}), reproduces the features of the Sb time-series observed in Exp. IV (Fig. 3: h). However, the failure of the model to account for Sb(III) accumulation in the solid phase is possibly related to the experimentally observed mismatch between Sb loss from solution and that accumulated in the solid-phase (18%) (Fig. A.1). In the presence of As(III) and As(V), the missing Sb could be volatilized via methylation (Hartmann et al., 2003). Overall, sensitivity analyses identify the rate of adsorption ($k_f^{Sb(OH)_6}$) as the most critical parameter controlling the mobility of Sb(V) in the argillaceous suspension (Fig. D.4).

4.2.4. Fate of Cr in the presence of microorganisms

Sequestration of Cr in the argillaceous suspensions likely proceeds via reductive precipitation of $Cr(OH)_{3(s)}$, which is enhanced in the presence of microorganisms in Exp. II – III as compared to abiotic Exp. I (Fig. 3: i-k). Similar to As and Sb, native microorganisms could induce Cr(VI) reduction via detoxification (Cheung and Gu, 2007). Reductive detoxification of both Cr and Sb may reflect a microbial strategy for metal sequestration via precipitation. Alternatively, Cr(VI) could be reduced via extracellular non-enzymatic processes. In this case bacteria could serve as electron donors after biosorption of Cr to the microbial cell wall (Viti et al., 2014). To account for the microbial control on Cr sequestration, we introduce a microbial pathway of Cr(VI) reduction to the model (Table 2, R^{29}).

In Exp. IV, rapid Cr removal during the first 3 days (Fig. 3: l) likely reflects the addition of soil inoculum capable of Cr respiration (Viti et al., 2014). We therefore, include Cr respiration (Chen and Hao, 1998) into the model (Table 2, R^{30}). Our estimate for the rate constant of reduction falls within the range reported for Cr(VI) reduction by dissimilatory iron-reducing bacteria (0.8×10^{-4} – 3.1×10^{-4} h^{-1}) (Table D.2) (Fendorf et al., 2000). Note that although some removal of aqueous Cr by mineral particles in the added soil inoculum cannot be excluded, we do not believe this is an important process. Sensitive model parameters include the maximum rate of detoxification ($r_{max}^{CrO_4^{2-}}$), as well as the rate constants of abiotic reduction ($k_{ab}^{CrO_4^{2-}}$), sorption ($k_f^{CrO_4^{2-}}$), and desorption ($k_b^{CrO_4^{2-}}$) (Fig. D.4). Consistent with the experimental observations, the model-predicted temporal changes of the aqueous Cr(VI) concentration is relatively insensitive to the value imposed for the O_2 inhibition constant ($K_{O_2}^{in}$).

4.3. Respiration versus detoxification

The experimental results provide evidence that the fate of the contaminant oxyanions (i.e., $HAsO_4^{2-}$, $Sb(OH)_6^-$, and CrO_4^{2-}) added to the argillaceous suspensions depends on the level of microbial activity (as inferred from NO_3^- and ATP data) and the microbial diversity and functionality (native versus inoculated consortia). The experimental results further suggest two distinct strategies employed by the microorganisms to deal with the mixed contaminants (Fig. 4).

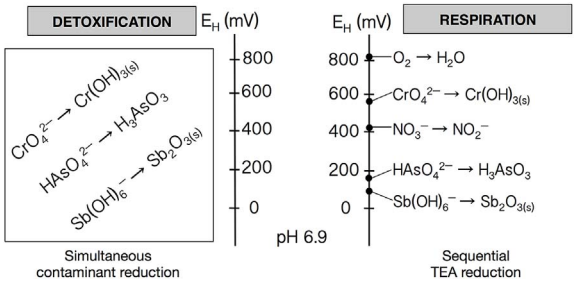

Fig. 4. Redox scale showing the theoretical succession of redox potentials (E_H in mV) calculated for the initial experimental conditions (pH 6.9, activities of oxidized and reduced species; Table 4). Potentially toxic CrO_4^{2-}, $HAsO_4^{2-}$, and $Sb(OH)_6^-$ can be reduced simultaneously, likely via detoxification, with no dependency on E_H (on the left) under aerobic and denitrifying conditions, or successively as terminal electron acceptors (TEAs) via respiration following the thermodynamic order (i.e., E_H cascade) (on the right). Note that NO_3^- is exclusively reduced via respiration in the presence of microorganisms.

The first strategy involves the simultaneous reduction of $HAsO_4^{2-}$, $Sb(OH)_6^-$, and CrO_4^{2-} under aerobic and denitrifying conditions. This is observed in the suspensions of Exp. II – III (Fig. 2: b-c). It is consistent with the previously observed simultaneous reduction of SO_4^{2-} and As (V) (Macy et al., 2000) or Fe(III) and As(V) (Smeaton et al., 2012), in which As is reduced as part of a detoxification pathway. Furthermore, the suggested detoxification mechanism may explain the bioreduction of other potentially toxic elements, for example U(VI), which can be reduced alongside of Fe(III) or SO_4^{2-} in sediments (Finneran et al., 2002; Komlos et al., 2008).

The second strategy involves the respiratory reduction of the oxyanions that follows the thermodynamic sequence from highest to lowest reduction potential (Table 4). Such a sequential reduction order is observed when the argillaceous suspensions are enriched with the soil inoculum in Exp. IV (Fig. 2: d). The corresponding sequence of TEA utilization in Exp. IV is then: O_2, CrO_4^{2-}, NO_3^-, $HAsO_4^{2-}$ and $Sb(OH)_6^-$.

4.4. Redox potential of the argillaceous suspension

Measured E_H values of the argillaceous suspensions during anoxic periods ($+283 \pm 65$ mV) do not correspond to the values predicted by the Nernst equation for the experimental conditions based on the redox couples: $CrO_4^{2-}/Cr(OH)_3$, NO_3^-/NO_2^-, $HAsO_4^{2-}/H_3AsO_3$ and $Sb(OH)_6^-/Sb_2O_{3(s)}$ (Table 4). Even though the activity ratios of the redox couples imply a range of redox conditions, from oxidizing (Exp. I) to reducing (Exp. II – IV), the measured E_H values do not respond quantitatively to these conditions and remain systematically above $+200$ mV. Therefore, the measurement of E_H does not yield a quantitative indicator of Cr, N, As, or Sb redox processes, most likely because none of the corresponding redox couples are electroactive towards the redox electrode (Markelova et al., 2017). Overall, our results confirm that E_H measurements are not particularly informative in environments depleted in electroactive redox couples (e.g., Fe couples), such as argillaceous formations.

4.5. Stability of reduced contaminants

We did not observe re-oxidation of reduced As(III), Sb(III) and Cr (III) during the oxic periods, even though oxidation of the reduced forms of these elements by O_2 is thermodynamically favorable under the experimental conditions (Campbell and Nordstrom, 2014). The

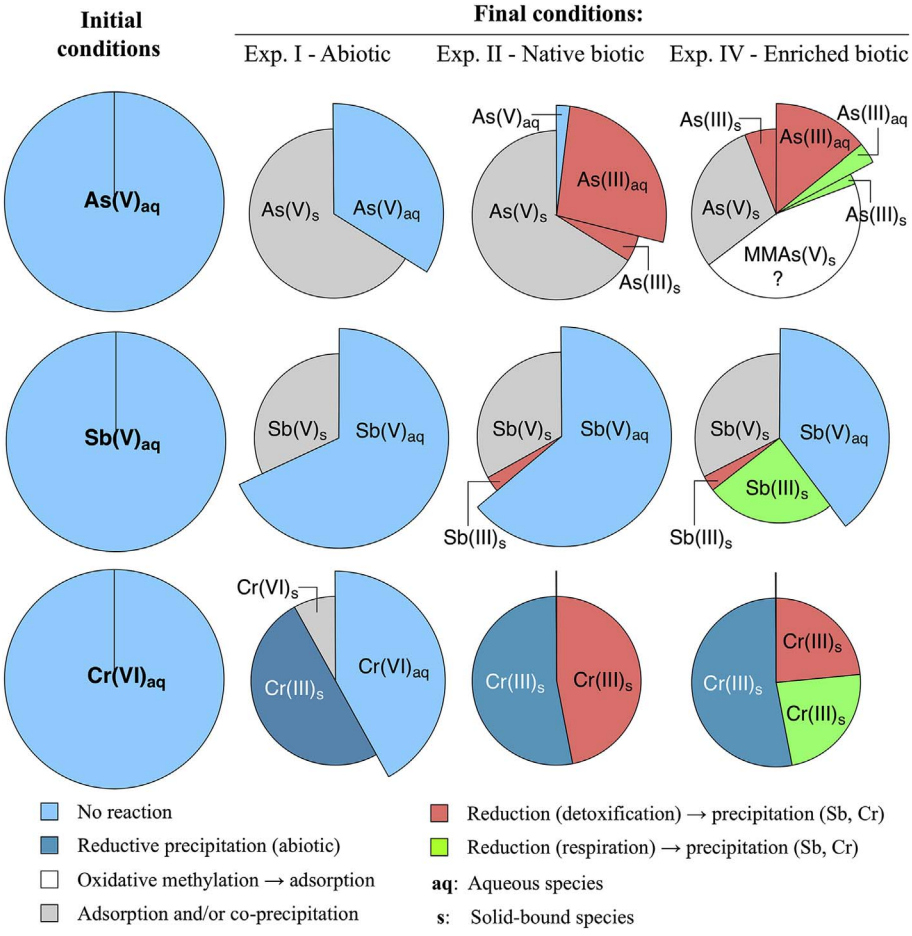

Fig. 5. Contribution of the various reaction pathways to the simultaneous sequestration of aqueous As(V), Sb(V), and Cr (VI) simulated by the model for the experimental end points. The results of Exp. III where the native microbial community was stimulated by the addition of organic carbon are similar to those of Exp. II within 5%, and are therefore not shown.

apparent stability of the reduced species observed here contrasts with previous studies of contaminant dynamics in topsoil suspensions under similar redox-oscillating conditions (e.g., Couture et al., 2015; Hockmann et al., 2014; Parsons et al., 2013), where re-oxidation is observed to various degrees. We hypothesize that the lack of re-oxidation reflects kinetic limitation in argillaceous materials lacking reactive Fe- and Mn-oxyhydroxides (Table A.2) (Leuz and Johnson, 2005; Rai et al., 1989). It is also possible that oxidizing microorganisms were not fully established in the reactor system due to the short experimental incubation period. These factors have all been previously linked to the re-oxidation of contaminants in soils (Buschmann et al., 2005; Butler et al., 2015; Hug and Leupin, 2003).

5. Conclusions

The fate of oxyanions of As(V), Sb(V) and Cr(VI) in Tégulines argillaceous suspensions was monitored under oscillating oxic-anoxic conditions in an increasing complexity experimental design using a bioreactor system. A dynamic modelling approach was used to reproduce the data and provide an internally consistent interpretation of the possible pathways responsible for the sequestration of the aqueous contaminants (Fig. 5, Table D.3). The modelling results suggest that a combination of adsorption, microbial detoxification and respiration processes explains the most extensive removal of As(V) from solution observed in Exp. IV. Moreover, we speculate that in Exp. IV, microbial methylation of As(III) to MMAs(V) may have prevented the accumulation of toxic As(III) in solution. In contrast to As, sequestration of aqueous Sb and Cr is mainly controlled by reductive precipitation, likely forming $Sb_2O_{3(s)}$ and $Cr(OH)_{3(s)}$. The reductive precipitation of Sb (III) appears to be mainly microbially mediated, contrary to Cr for which abiotic reductive precipitation is identified as the major sequestration pathway under all investigated conditions. We further propose that the ability of the native microbial community to simultaneously reduce oxidized As, Sb and Cr, irrespective of the thermodynamically predicted order and independent of the availability of dissolved organic carbon, may be diagnostic of contaminant detoxification (Exp. II – III). In contrast, a sequence of contaminant reduction reactions that follows the order of decreasing redox potentials of electron acceptors (in Exp. IV: O_2, CrO_4^{2-}, NO_3^-, $HAsO_4^{2-}$, $Sb(OH)_6^-$) is suggestive of respiration rather than detoxification. Keeping in mind that we only considered short-termed oxidative perturbations (7 days), our experimental and modelling results indicate that the investigated argillaceous formation may constitute a suitable geochemical environment for contaminant sequestration, as exposure to O_2 did not cause the re-release of the contaminants to the aqueous phase. This conclusion, however, will have to be confirmed for redox oscillations lasting on longer time scales (e.g., several months and longer).

Acknowledgments

We acknowledge Delphine Tisserand (University of Georgia) and Marianne Vandergriendt (University of Waterloo) for support in the laboratory. We are grateful to Nele Bleyen and Hugo Moors from SCK-CEN for helpful discussions on the geomicrobiology of the argillaceous formations. We appreciate a detailed feedback of Grant Ferris to this work reviewed as part of EM's PhD thesis. This research was funded by Andra (the French National Radioactive Waste Management Agency), the Geochemistry group at ISTerre, which is a part of Labex OSUG@ 2020 (ANR 10 LABX 56), and the Canada Excellence Research Chair program.

Appendix A. Supplementary data

Supplementary data related to this article can be found at http://dx.doi.org/10.1016/j.apgeochem.2017.12.012.

References

Abin, C.A., Hollibaugh, J.T., 2014. Dissimilatory antimonate reduction and production of antimony trioxide microcrystals by a novel microorganism. Environ. Sci. Technol. 48, 681–688. http://dx.doi.org/10.1021/es404098z.

Andra, 2009. French National Plan for the Management of Radioactive Materials and Waste (PNGMDR).

Andrewes, P., Cullen, W.R., Polishchuk, E., 2000. Arsenic and antimony biomethylation by Scopulariopsis brevicaulis: interaction of arsenic and antimony compounds. Environ. Sci. Technol. 34, 2249–2253. http://dx.doi.org/10.1021/es991269p.

Appelo, C.A.J., Postma, D., 2005. Geochemistry, Groundwater and Pollution. CRC Press LLC.

Bard, J.A., Parsons, R., Jordan, J., 1985. Standard Potentials in Aqueous Solution. Marcel Dekker, Inc.

Bergmann, J., Friedel, P., Kleeberg, R., 1998. BGMN - a new fundamental parameters based Rietveld program for laboratory X-ray sources, it's use in quantitative analysis and structure investigations. Comm. Powder Diffraction, Int. Union Crystallogr. CPD Newsl. 20, 5–8.

Bertron, A., Jacquemet, N., Erable, B., Sablayrolles, C., Escadeillas, G., Albrecht, A., 2014. Reactivity of nitrate and organic acids at the concrete–bitumen interface of a nuclear waste repository cell. Nucl. Eng. Des. 268, 51–57. http://dx.doi.org/10.1016/j.nucengdes.2013.11.085.

Bildstein, O., Pozo, C., Jullien, M., Trotignon, L., 2005. Modelling oxidising perturbations in argillaceous material. In: Clays in Natural and Engineered Barriers for Radioactive Waste Confinement Meeting. 14–18/03, Tours, France.

Bosch, J., Lee, K.-Y., Jordan, G., Kim, K.-W., Meckenstock, R.U., 2012. Anaerobic, nitrate-dependent oxidation of pyrite nanoparticles by Thiobacillus denitrificans. Environ. Sci. Technol. 46, 2095–2101. http://dx.doi.org/10.1021/es2022329.

Bothe, J.V., Brown, P.W., 1999. The stabilities of calcium arsenates at 23 ± 1°C. J. Hazard Mater. 69, 197–207. http://dx.doi.org/10.1016/S0304-3894(99)00105-3.

Buschmann, J., Canonica, S., Sigg, L., 2005. Photoinduced oxidation of antimony(III) in the presence of humic acid. Environ. Sci. Technol. 39, 5335–5341. http://dx.doi.org/10.1021/es050269o.

Butler, E.C., Chen, L., Hansel, C.M., Krumholz, L.R., Elwood Madden, A.S., Lan, Y., 2015. Biological versus mineralogical chromium reduction: potential for reoxidation by manganese oxide. Environ. Sci. Process. Impacts 17, 1930–1940. http://dx.doi.org/10.1039/C5EM00286A.

Campbell, K.M., Nordstrom, D.K., 2014. Arsenic speciation and sorption in natural environments. Rev. Mineral. Geochem. 79, 185–216. http://dx.doi.org/10.2138/rmg.2014.79.3.

Casiot, C., Ujevic, M., Munoz, M., Seidel, J.L., Elbaz-Poulichet, F., 2007. Antimony and arsenic mobility in a creek draining an antimony mine abandoned 85 years ago (upper Orb basin, France). Appl. Geochem. 22, 788–798. http://dx.doi.org/10.1016/j.apgeochem.2006.11.007.

Chakraborty, S., Wolthers, M., Chatterjee, D., Charlet, L., 2007. Adsorption of arsenite and arsenate onto muscovite and biotite mica. J. Colloid Interface Sci. 309, 392–401. http://dx.doi.org/10.1016/j.jcis.2006.10.014.

Charlet, L., Bardelli, F., Parsons, C.T., He, J., Chakraborty, S., Gailer, J., 2012. Arsenic binding onto phyllosilicates and glutathione: soil immobilisation and human excretion mechanisms. In: Noller, Ng, Naidu, Bundschuh, Bhattacharya (Eds.), Understanding the Geological and Medical Interface of Arsenic. Taylor & Francis Group, London, pp. 59–62.

Chen, J.M., Hao, O.J., 1998. Microbial chromium (VI) reduction. Crit. Rev. Environ. Sci. Technol. 28, 219–251. http://dx.doi.org/10.1080/10643389891254214.

Cheung, K.H., Gu, J., 2007. Mechanism of hexavalent chromium detoxification by microorganisms and bioremediation application potential: a review. Int. Biodeterior. Biodegrad. 59, 8–15. http://dx.doi.org/10.1016/j.ibiod.2006.05.002.

Chon, C.-M., Kim, J.G., Moon, H.-S., 2006. Kinetics of chromate reduction by pyrite and biotite under acidic conditions. Appl. Geochem. 21, 1469–1481. http://dx.doi.org/10.1016/j.apgeochem.2006.06.012.

Cornelis, G., Johnson, C.A., Gerven, T. Van, Vandecasteele, C., 2008. Leaching mechanisms of oxyanionic metalloid and metal species in alkaline solid wastes: a review. Appl. Geochem. 23, 955–976. http://dx.doi.org/10.1016/j.apgeochem.2008.02.001.

Cory, R.M., McKnight, D.M., 2005. Fluorescence spectroscopy reveals ubiquitous presence of oxidized and reduced quinones in dissolved organic matter. Environ. Sci. Technol. 39, 8142–8149. http://dx.doi.org/10.1021/es0506962.

Cotten, J., Le Dez, A., Bau, M., Caroff, M., Maury, R.C., Dulski, P., Fourcade, S., Bohn, M., Brousse, R., 1995. Origin of anomalous rare-earth element and yttrium enrichments in subaerially exposed basalts: evidence from French Polynesia. Chem. Geol. 119, 115–138. http://dx.doi.org/10.1016/0009-2541(94)00102-E.

Couture, R.-M., Rose, J., Kumar, N., Mitchell, K., Wallschläger, D., Van Cappellen, P., 2013. Sorption of arsenite, arsenate, and thioarsenates to iron oxides and iron sulfides: a kinetic and spectroscopic investigation. Environ. Sci. Technol. 47, 5652–5659. http://dx.doi.org/10.1021/es3049724.

Couture, R.-M., Charlet, L., Markelova, E., Madé, B., Parsons, C.T., 2015. On–off mobilization of contaminants in soils during redox oscillations. Environ. Sci. Technol. 49, 3015–3023. http://dx.doi.org/10.1021/es5061879.

Dovick, M.A., Kulp, T.R., Arkle, R.S., Pilliod, D.S., 2016. Bioaccumulation trends of arsenic and antimony in a freshwater ecosystem affected by mine drainage. Environ. Chem. 13, 149. http://dx.doi.org/10.1071/EN15046.

Duro, L., Domènech, C., Grivé, M., Roman-Ross, G., Bruno, J., Källström, K., 2014. Assessment of the evolution of the redox conditions in a low and intermediate level nuclear waste repository (SFR1, Sweden). Appl. Geochem. 49, 192–205. http://dx.doi.org/10.1016/j.apgeochem.2014.04.015.

Fawcett, S.E., Jamieson, H.E., Nordstrom, D.K., McCleskey, R.B., 2015. Arsenic and

antimony geochemistry of mine wastes, associated waters and sediments at the Giant Mine, Yellowknife, Northwest Territories, Canada. Appl. Geochem. 62, 3–17. http://dx.doi.org/10.1016/j.apgeochem.2014.12.012.
Fendorf, S., Wielinga, B.W., Hansel, C.M., 2000. Chromium transformations in natural environments: the role of biological and abiological processes in chromium(VI) reduction. Int. Geol. Rev. 42, 691–701. http://dx.doi.org/10.1080/00206810009465107.
Filella, M., May, P.M., 2003. Computer simulation of the low-molecular-weight inorganic species distribution of antimony(III) and antimony(V) in natural waters. Geochem. Cosmochim. Acta 67, 4013–4031. http://dx.doi.org/10.1016/S0016-7037(03)00095-4.
Finneran, K.T., Housewright, M.E., Lovley, D.R., 2002. Multiple influences of nitrate on uranium solubility during bioremediation of uranium-contaminated subsurface sediments. Environ. Microbiol. 4, 510–516. http://dx.doi.org/10.1046/j.1462-2920.2002.00317.x.
Gallegos, T.J., Hyun, S.P., Hayes, K.F., 2007. Spectroscopic investigation of the uptake of arsenite from solution by synthetic mackinawite. Environ. Sci. Technol. 41, 7781–7786. http://dx.doi.org/10.1021/es070613c.
Gaucher, E.C., Tournassat, C., Pearson, F.J., Blanc, P., Crouzet, C., Lerouge, C., Altmann, S., 2009. A robust model for pore-water chemistry of clayrock. Geochim. Cosmochim. Acta 73, 6470–6487. http://dx.doi.org/10.1016/j.gca.2009.07.021.
Ghorbanzadeh, N., Lakzian, A., Halajnia, A., Kabra, A.N., Kurade, M.B., Lee, D.S., Jeon, B.-H., 2015. Influence of clay minerals on sorption and bioreduction of arsenic under anoxic conditions. Environ. Geochem. Health 37, 997–1005. http://dx.doi.org/10.1007/s10653-015-9708-x.
Godgul, G., Sahu, K.C., 1995. Chromium contamination from chromite mine. Environ. Geol. 25, 251–257. http://dx.doi.org/10.1007/BF00766754.
Gorny, J., Billon, G., Lesven, L., Dumoulin, D., Madé, B., Noiriel, C., 2015. Arsenic behavior in river sediments under redox gradient: a review. Sci. Total Environ. 505, 423–434. http://dx.doi.org/10.1016/j.scitotenv.2014.10.011.
Hallbeck, L., Pedersen, K., 2012. Culture-dependent comparison of microbial diversity in deep granitic groundwater from two sites considered for a Swedish final repository of spent nuclear fuel. FEMS Microbiol. Ecol. 81, 66–77. http://dx.doi.org/10.1111/j.1574-6941.2011.01281.x.
Hammes, F., Goldschmidt, F., Vital, M., Wang, Y., Egli, T., 2010. Measurement and interpretation of microbial adenosine tri-phosphate (ATP) in aquatic environments. Water Res. 44, 3915–3923. http://dx.doi.org/10.1016/j.watres.2010.04.015.
Hartmann, L.M., Craig, P.J., Jenkins, R.O., 2003. Influence of arsenic on antimony methylation by the aerobic yeast Cryptococcus humicolus. Arch. Microbiol. 180, 347–352. http://dx.doi.org/10.1007/s00203-003-0600-1.
Hedin, A., Olsson, O., 2016. Crystalline rock as a repository for Swedish spent nuclear fuel. Elements 12, 247–252. http://dx.doi.org/10.2113/gselements.12.4.247.
Herman, J., Usher, W., 2017. SALib: an open-source Python library for sensitivity analysis. J. Open Source Softw 2. https://doi.org/10.21105/joss.00097.
Hindersmann, I., Mansfeldt, T., 2014. Trace element solubility in a multimetal-contaminated soil as affected by redox conditions. Water Air Soil Pollut. 225, 2158. http://dx.doi.org/10.1007/s11270-014-2158-8.
Hockmann, K., Lenz, M., Tandy, S., Nachtegaal, M., Janousch, M., Schulin, R., 2014. Release of antimony from contaminated soil induced by redox changes. J. Hazard Mater. 275, 215–221. http://dx.doi.org/10.1016/j.jhazmat.2014.04.065.
Hug, S.J., Leupin, O., 2003. Iron-catalyzed oxidation of arsenic(III) by oxygen and by hydrogen peroxide: pH-dependent formation of oxidants in the fenton reaction. Environ. Sci. Technol. 37, 2734–2742. http://dx.doi.org/10.1021/es026208x.
Ilgen, A.G., Majs, F., Barker, A.J., Douglas, T.A., Trainor, T.P., 2014. Oxidation and mobilization of metallic antimony in aqueous systems with simulated groundwater. Geochem. Cosmochim. Acta 132, 16–30. http://dx.doi.org/10.1016/j.gca.2014.01.019.
Jackson, M.L., Lim, C.H., Zelazny, L.W., 1986. Oxides, hydroxides, and aluminosilicates. In: Klute, A. (Ed.), Methods of Soil Analysis Part 1, pp. 101–150.
Jamieson-Hanes, J.H., Gibson, B.D., Lindsay, M.B.J., Kim, Y., Ptacek, C.J., Blowes, D.W., 2012. Chromium isotope fractionation during reduction of Cr(VI) under saturated flow conditions. Environ. Sci. Technol. 46, 6783–6789. http://dx.doi.org/10.1021/es2042383.
Johnson, C.A., Moench, H., Wersin, P., Kugler, P., Wenger, C., 2005. Solubility of antimony and other elements in samples taken from shooting ranges. J. Environ. Qual. 34, 248–254.
Jones, E., Oliphant, T., Peterson, P., 2001. SciPy: Open Source Scientific Tools for Python.
Karl, D.M., 1980. Cellular nucleotide measurements and applications in microbial ecology. Microbiol. Rev. 44, 739–796 doi:0146-0749/80/04-0739/58.
Komlos, J., Moon, H.S., Jaffé, P.R., 2008. Effect of sulfate on the simultaneous bioreduction of iron and uranium. J. Environ. Qual. 37, 2058. http://dx.doi.org/10.2134/jeq2007.0665.
Konhauser, K.O., 2007. Introduction to Geomicrobiology. Blackwell Science.
Kulp, T.R., Miller, L.G., Braiotta, F., Webb, S.M., Kocar, B.D., Blum, J.S., Oremland, R.S., 2014. Microbiological reduction of Sb(V) in anoxic freshwater sediments. Environ. Sci. Technol. 48, 218–226. http://dx.doi.org/10.1021/es403312j.
Laaksoharju, M., Smellie, J., Tullborg, E.-L., Gimeno, M., Molinero, J., Gurban, I., Hallbeck, L., 2008. Hydrogeochemical evaluation and modelling performed within the Swedish site investigation programme. Appl. Geochem. 23, 1761–1795. http://dx.doi.org/10.1016/j.apgeochem.2008.02.015.
Lafferty, B.J., Loeppert, R.H., 2005. Methyl arsenic adsorption and desorption behavior on iron oxides. Environ. Sci. Technol. 34, 3131–3136. http://dx.doi.org/10.1021/es048701+.
Lan, Y., Li, C., Mao, J., Sun, J., 2008. Influence of clay minerals on the reduction of Cr6+ by citric acid. Chemosphere 71, 781–787. http://dx.doi.org/10.1016/j.chemosphere.2007.10.010.
Leuz, A.-K., Johnson, C.A., 2005. Oxidation of Sb(III) to Sb(V) by O2 and H2O2 in aqueous solutions. Geochem. Cosmochim. Acta 69, 1165–1172. http://dx.doi.org/10.1016/j.gca.2004.08.019.
Lin, Z., Puls, R.W., 2000. Adsorption, desorption and oxidation of arsenic affected by clay minerals and aging process. Environ. Geol. 39, 753–759. http://dx.doi.org/10.1007/s002540050490.
Lindsay, M.B.J., Blowes, D.W., Condon, P.D., Ptacek, C.J., 2011. Organic carbon amendments for passive in situ treatment of mine drainage: field experiments. Appl. Geochem. 26, 1169–1183. http://dx.doi.org/10.1016/j.apgeochem.2011.04.006.
Lintschinger, J., Koch, I., Serves, S., Feldmann, J., Cullen, W.R., 1997. Determination of antimony species with high-performance liquid chromatography using element specific detection. Fresen. J. Anal. Chem. 359, 484–491. http://dx.doi.org/10.1007/s002160050618.
Lloyd, J.R., Oremland, R.S., 2006. Microbial transformations of arsenic in the environment: from soda lakes to aquifers. Elements 2, 85–90. http://dx.doi.org/10.2113/gselements.2.2.85.
Macy, J.M., Santini, J.M., Pauling, B.V., O'Neill, A.H., Sly, L.I., 2000. Two new arsenate/sulfate-reducing bacteria: mechanisms of arsenate reduction. Arch. Microbiol. 173, 49–57. http://dx.doi.org/10.1007/s002030050007.
Manning, B.A., Goldberg, S., 1997. Adsorption and stability of arsenic(III) at the clay mineral − water interface. Environ. Sci. Technol. 31, 2005–2011. http://dx.doi.org/10.1021/es9608104.
Markelova, E., Parsons, C.T., Couture, R.-M., Smeaton, C.M., Madé, B., Charlet, L., Van Cappellen, P., 2017. Deconstructing the redox cascade: what role do microbial exudates (flavins) play? Environ. Chem Registered number: EN17158, Accepted 08 November 2017.
Matern, K., Mansfeldt, T., 2016. Chromium release from a COPR-contaminated soil at varying water content and redox conditions. J. Environ. Qual. 45, 1259. http://dx.doi.org/10.2134/jeq2015.10.0506.
Mestrot, A., Planer-Friedrich, B., Feldmann, J., 2013. Biovolatilisation: a poorly studied pathway of the arsenic biogeochemical cycle. Environ. Sci. Process. Impacts 15, 1639. http://dx.doi.org/10.1039/c3em00105a.
Mitsunobu, S., Harada, T., Takahashi, Y., 2006. Comparison of antimony behavior with that of arsenic under various soil redox conditions. Environ. Sci. Technol. 40, 7270–7276. http://dx.doi.org/10.1021/es060694x.
Nagra, 2002. Demonstration of disposal feasibility for spent fuel, vitrified high-level waste and long-lived intermediate-level waste. NAGRA Technical Report NTB 02–05.
Nordstrom, D.K., Majzlan, J., Konigsberger, E., 2014. Thermodynamic properties for arsenic minerals and aqueous species. Rev. Mineral. Geochem. 79, 217–255. http://dx.doi.org/10.2138/rmg.2014.79.4.
Nriagu, J., Beaubien, S., Blowes, D., 1993. Chemistry of chromium in lakes. Environ. Rev. 1, 104–120. http://dx.doi.org/10.1139/a93-009.
Nuclear Energy Agency, 1958. Clay Club. https://www.oecd-nea.org, Accessed date: 25 November 2016.
Oremland, R.S., 2005. A microbial arsenic cycle in a salt-saturated, extreme environment. Science (80-.) 308, 1305–1308. http://dx.doi.org/10.1126/science.1110832.
Oremland, R.S., Saltikov, C.W., Wolfe-Simon, F., Stolz, J.F., 2009. Arsenic in the evolution of earth and extraterrestrial ecosystems. Geomicrobiol. J. 26, 522–536. http://dx.doi.org/10.1080/01490450903102525.
Panichev, N., Mandiwana, K., Kataeva, M., Siebert, S., 2005. Determination of Cr(VI) in plants by electrothermal atomic absorption spectrometry after leaching with sodium carbonate. Spectrochim. Acta Part B At. Spectrosc. 60, 699–703. http://dx.doi.org/10.1016/j.sab.2005.02.018.
Parkhurst, D.L., Appelo, C.A., 2013. Description of input and examples for PHREEQC version 3 – a computer program for speciation, batch-reaction, one-dimensional transport, and inverse geochemical calculations. U.S. Geol. Surv. Tech. Methods 6, 497.
Parsons, C.T., Couture, R.-M., Omoregie, E.O., Bardelli, F., Greneche, J.-M., Roman-Ross, G., Charlet, L., 2013. The impact of oscillating redox conditions: arsenic immobilisation in contaminated calcareous floodplain soils. Environ. Pollut. 178, 254–263. http://dx.doi.org/10.1016/j.envpol.2013.02.028.
Pedersen, K., 2002. Chapter 10 Microbial processes in the disposal of high level radioactive waste 500 m underground in Fennoscandian Shield rocks. In: Interactions of Microorganisms with Radionuclides, pp. 279–311. http://dx.doi.org/10.1016/S1569-4860(02)80039-0.
Plant, J.A., Kinniburgh, D.G., Smedley, P.L., Fordyce, F.M., Klinck, B.A., 2005. Arsenic and selenium. In: Lollar, B.S. (Ed.), Environmental Geochemistry. British Geological Survey. Keyworth, Nottingham, UK.
Rai, D., Eary, L.E., Zachara, J.M., 1989. Environmental chemistry of chromium. Sci. Total Environ. 86, 15–23. http://dx.doi.org/10.1016/0048-9697(89)90189-7.
Rai, D., Moore, D. a., Hess, N.J., Rosso, K.M., Rao, L., Heald, S.M., 2007. Chromium(III) hydroxide solubility in the aqueous K+-H+-OH−-CO2-HCO3−-CO32−-H2O system: a thermodynamic model. J. Solut. Chem. 36, 1261–1285. http://dx.doi.org/10.1007/s10953-007-9179-5.
Rakshit, S., Sarkar, D., Datta, R., 2015. Surface complexation of antimony on kaolinite. Chemosphere 119, 349–354. http://dx.doi.org/10.1016/j.chemosphere.2014.06.070.
Raposo, J.C., Zuloaga, O., Olazabal, M.A., Madariaga, J.M., 2004. Study of the precipitation equilibria of arsenate anion with calcium and magnesium in sodium perchlorate at 25 °C. Appl. Geochem. 19, 855–862. http://dx.doi.org/10.1016/j.apgeochem.2003.10.012.
Rivett, M.O., Buss, S.R., Morgan, P., Smith, J.W.N., Bemment, C.D., 2008. Nitrate attenuation in groundwater: a review of biogeochemical controlling processes. Water Res. 42, 4215–4232. http://dx.doi.org/10.1016/j.watres.2008.07.020.
Rodwell, W., Norris, S., Cool, W., Cunado, M., et al., 2003. A Thematic Network on Gas Issues in Safety Assessment of Deep Repositories for Radioactive Waste (GASNET).

Roig-Navarro, A., Martinez-Bravo, Y., López, F., Hernández, F., 2001. Simultaneous determination of arsenic species and chromium(VI) by high-performance liquid chromatography–inductively coupled plasma-mass spectrometry. J. Chromatogr. A 912, 319–327. http://dx.doi.org/10.1016/S0021-9673(01)00572-6.

Saltelli, A., Tarantola, S., Chan, K.P.-S., 1999. A quantitative model-independent method for global sensitivity analysis of model output. Technometrics 41, 39–56. http://dx.doi.org/10.1080/00401706.1999.10485594.

Saltikov, C.W., Wildman, R.A., Newman, D.K., 2005. Expression dynamics of arsenic respiration and detoxification in Shewanella sp. strain ANA-3. J. Bacteriol. 187, 7390–7396. http://dx.doi.org/10.1128/JB.187.21.7390-7396.2005.

Scott, N., Hatlelid, K.M., MacKenzie, N.E., Carter, D.E., 1993. Reactions of arsenic(III) and arsenic(V) species with glutathione. Chem. Res. Toxicol. 6, 102–106. http://dx.doi.org/10.1021/tx00031a016.

Sharma, P., Kappler, A., 2011. Desorption of arsenic from clay and humic acid-coated clay by dissolved phosphate and silicate. J. Contam. Hydrol. 126, 216–225. http://dx.doi.org/10.1016/j.jconhyd.2011.08.005.

Silver, S., Phung, L.T., 2005. Genes and enzymes involved in bacterial oxidation and reduction of inorganic arsenic. Appl. Environ. Microbiol. 71, 599–608. http://dx.doi.org/10.1128/AEM.71.2.599-608.2005.

Small, J., Nykyri, M., Helin, M., Hovi, U., Sarlin, T., Itävaara, M., 2008. Experimental and modelling investigations of the biogeochemistry of gas production from low and intermediate level radioactive waste. Appl. Geochem. 23, 1383–1418. http://dx.doi.org/10.1016/j.apgeochem.2007.11.020.

Smeaton, C.M., Walshe, G.E., Smith, A.M.L., Hudson-Edwards, K.A., Dubbin, W.E., Wright, K., Beale, A.M., Fryer, B.J., Weisener, C.G., 2012. Simultaneous release of Fe and as during the reductive dissolution of Pb–As jarosite by *Shewanella putrefaciens* CN32. Environ. Sci. Technol. 46, 12823–12831. http://dx.doi.org/10.1021/es3021809.

Sø, H.U., Postma, D., Jakobsen, R., Larsen, F., 2008. Sorption and desorption of arsenate and arsenite on calcite. Geochem. Cosmochim. Acta 72, 5871–5884. http://dx.doi.org/10.1016/j.gca.2008.09.023.

Song, C., Zhang, J., 2008. Electrocatalytic oxygen reduction reaction. In: Zhang, J. (Ed.), (Ed.), PEM Fuel Cell Electrocatalysts and Catalyst Layers: Fundamentals and Applications. Springer, pp. 89–134. http://dx.doi.org/10.1007/978-1-84800-936-3_2.

Stewart, B.D., Nico, P.S., Fendorf, S., 2009. Stability of uranium incorporated into Fe (hydr)oxides under fluctuating redox conditions. Environ. Sci. Technol. 43, 4922–4927. http://dx.doi.org/10.1021/es803317w.

Stroes-Gascoyne, S., Hamon, C.J., Vilks, P., Gierszewski, P., 2002. Microbial, redox and organic characteristics of compacted clay-based buffer after 6.5 years of burial at AECL's Underground Research Laboratory. Appl. Geochem. 17, 1287–1303. http://dx.doi.org/10.1016/S0883-2927(02)00020-3.

Stucker, V.K., Silverman, D.R., Williams, K.H., Sharp, J.O., Ranville, J.F., 2014. Thioarsenic species associated with increased arsenic release during biostimulated subsurface sulfate reduction. Environ. Sci. Technol. 48, 13367–13375. http://dx.doi.org/10.1021/es5035206.

Swift, P.N., Bonano, E.J., 2016. Geological disposal of nuclear waste in tuff: Yucca Mountain (USA). Elements 12, 263–268. http://dx.doi.org/10.2113/gselements.12.4.263.

Thompson, A., Chadwick, O.A., Rancourt, D.G., Chorover, J., 2006. Iron-oxide crystallinity increases during soil redox oscillations. Geochem. Cosmochim. Acta 70, 1710–1727. http://dx.doi.org/10.1016/j.gca.2005.12.005.

Tournassat, C., Gaucher, E.C., Fattahi, M., Grambow, B., 2007. On the mobility and potential retention of iodine in the Callovian–Oxfordian formation. Phys. Chem. Earth, Parts A/B/C 32, 539–551. http://dx.doi.org/10.1016/j.pce.2005.12.004.

Tratnyek, P.G., Macalady, D.L., 2000. Oxidation-reduction reactions in the aquatic environment. In: Boethling, R.S., Mackay, D. (Eds.), Handbook of Property Estimation Methods for Chemicals. CRC Press LLC, pp. 383–415.

Van Cappellen, P., Wang, Y., 1996. Cycling of iron and manganese in surface sediments; a general theory for the coupled transport and reaction of carbon, oxygen, nitrogen, sulfur, iron, and manganese. Am. J. Sci. 296, 197–243. http://dx.doi.org/10.2475/ajs.296.3.197.

Viti, C., Marchi, E., Decorosi, F., Giovannetti, L., 2014. Molecular mechanisms of Cr(VI) resistance in bacteria and fungi. FEMS Microbiol. Rev. 38, 633–659. http://dx.doi.org/10.1111/1574-6976.12051.

Wersin, P., Leupin, O.X., Mettler, S., Gaucher, E.C., Mäder, U., De Cannière, P., Vinsot, A., Gäbler, H.E., Kunimaro, T., Kiho, K., Eichinger, L., 2011. Biogeochemical processes in a clay formation in situ experiment: Part A – overview, experimental design and water data of an experiment in the Opalinus Clay at the Mont Terri Underground Research Laboratory, Switzerland. Appl. Geochem. 26, 931–953. http://dx.doi.org/10.1016/j.apgeochem.2011.03.004.

Willis, S.S., Haque, S.E., Johannesson, K.H., 2011. Arsenic and antimony in groundwater flow systems: a comparative study. Aquat. Geochem. 17, 775–807. http://dx.doi.org/10.1007/s10498-011-9131-6.

Wilson, S.C., Lockwood, P.V., Ashley, P.M., Tighe, M., 2010. The chemistry and behaviour of antimony in the soil environment with comparisons to arsenic: a critical review. Environ. Pollut. 158, 1169–1181. http://dx.doi.org/10.1016/j.envpol.2009.10.045.

Wu, W.-M., Carley, J., Luo, J., Ginder-Vogel, M. a., Cardenas, E., Leigh, M.B., Hwang, C., Kelly, S.D., Ruan, C., Wu, L., Van Nostrand, J., Gentry, T., Lowe, K., Carroll, S., Luo, W., Fields, M.W., Gu, B., Watson, D., Kemner, K.M., Marsh, T., Tiedje, J., Zhou, J., Fendorf, S., Kitanidis, P.K., Jardine, P.M., Criddle, C.S., 2007. In situ bioreduction of uranium (VI) to submicromolar levels and reoxidation by dissolved oxygen. Environ. Sci. Technol. 41, 5716–5723. http://dx.doi.org/10.1021/es062657b.

Xi, J., He, M., Lin, C., 2010. Adsorption of antimony(V) on kaolinite as a function of pH, ionic strength and humic acid. Environ. Earth Sci. 60, 715–722. http://dx.doi.org/10.1007/s12665-009-0209-z.

Zhang, H., Selim, H.M., 2005. Kinetics of arsenate adsorption – desorption in soils. Environ. Sci. Technol. 39, 6101–6108. http://dx.doi.org/10.1021/es050334u.

Zhang, J., Stanforth, R., 2005. Slow adsorption reaction between arsenic species and goethite (α-FeOOH): diffusion or heterogeneous surface reaction control. Langmuir 21, 2895–2901. http://dx.doi.org/10.1021/la047636e.

Zotov, a. V., Shikina, N.D., Akinfiev, N.N., 2003. Thermodynamic properties of the Sb(III) hydroxide complex Sb(OH)3(aq) at hydrothermal conditions. Geochem. Cosmochim. Acta 67, 1821–1836. http://dx.doi.org/10.1016/S0016-7037(00)01281-4.

Zydorczak, B., May, P.M., Meyrick, D.P., Bátka, D., Hefter, G., 2012. Dissolution of Cr2O3(s) and the behavior of chromium in concentrated NaOH solutions. Ind. Eng. Chem. Res. 51, 16537–16543. http://dx.doi.org/10.1021/ie302096e.